Università degli Studi di Padova

Dipartimento di Ingegneria Industriale

Corso di Laurea in Ingegneria Elettrica

Uncertainty Quantification for Superconducting Radio Frequency Single-Cell Cavities using Probability Sampling Methods

Relatore
Prof. Dr. Piergiorgio Alotto
Co-relatore
Prof. Dr. Ursula van Rienen

Laureando
Emanuele Brentegani

Contents

Abstract

Superconducting Radio Frequency cavities play a key role in particle accelerators. The effect of the uncertainty in the real-life geometry of the Superconducting niobium cavities is non-trivial; in this work we study its effect on certain parameters (i.e. the R/Q and the frequency) of the TM_{010} and TM_{110} modes of the TESLA Single-cell cavity. This is done by performing Uncertainty Quantification with replicated Latin Hypercube Sampling (rLHS). A linear fit of the sampling was also performed, as the coefficients of the approximating model provide measures of how much a certain geometric input parameter is capable of influencing the cavity properties. The whole study was done on the untuned cavity, and by considering only rotationally symmetric deviations. The results are consistent with what can be found in previous works of other authors.

Chapter 1

Introduction

Nowadays Radio Frequency(RF) Superconducting cavities are widely employed in particle accelerators.

The working principle of a RF accelerating cavity is the interaction between a particle beam and an electromagnetic standing wave located inside the cavity. When the device is transversed by a particle beam the electric field, tuned at a certain frequency, provides energy to the bunch.

The accelerating structures can be very complicated and are connected by the so called "beam pipes" which also allow the beam to enter different devices without exiting from the pumped vacuum region; in this framework, a huge problem can be represented by the interactions between the beam and the surrounding environment. For instance, the bunch can be significantly disrupted every time the change in the surrounding structures is not mild enough.

Normal conducting cavities are affected by great power losses, due to the current induced by the electromagnetic fields on their surfaces. Their design is therefore also targeted at limiting these losses and this leads to cavity shapes that represent extreme changes in the accelerating structures.

Superconducting cavities instead have nearly zero resistivity and allow to save huge amounts of power. For this reason their shape is smoother and the beam ports are usually larger than what is required by a normal conducting cavity ([1]). In this work we studied the superconducting TESLA single-cell cavity, which is an element of a periodic structure, the TESLA 9-cell cavity; it is manufactured in niobium and usually operated at a temperature of 2K.

Unfortunately the manufacturing of niobium cavities is more challenging than the one of normal conducting cavities. This is mainly due to the mechanical properties of niobium, and leads to cavities that present deviations from the design specifications in the lower millimeter range [2].

Thus an important question is how much the electromagnetic properties can differ from the designed specifications.

The purpose of this work is to study the effect of the geometric uncer-

tainties of the TESLA Single-cell cavity and see how they reflect on the eigenfrequency and the R/Q (for the definition of the R/Q see section 2.1.3) of the TM_{010} and TM_{110} eignemodes. This means performing uncertainty quantification.

Furthermore sensitivity analysis was applied, in order to understand which geometric parameters are the main responsible for the deviation of the considered cavity properties.

Some results on this topic were already available at the time of writing, as it will be seen in [2]. Nevertheless all of them refer only to the TM_{010} mode; whereas, as already explained, we developed a study also for the effect of the uncertainties on the mode TM_{110} .

Chapter 2

Cavity resonators

The purpose of this chapter is to describe the mathematical model that is applied to solve the physical problem of the electromagnetic field in a cavity. What is contained here has a more general validity and may obviously be applied to all the cavities that satisfy the hypothesis that are provided in the following pages.

2.1 Eigenmode decomposition

2.1.1 Wave equation

From a physical point of view, a cavity resonator is simply a portion of space bounded by a highly conductive surface. On that surface there may also be some holes which serve different purposes. Formally, a cavity resonator is modeled as a boundary value problem described by Maxwell's equations and the boundary conditions define the geometry and the interactions of the cavity with the external space. The space inside the cavity is assumed to be empty, therefore the magnetic permeability and the electric permittivity of free space are considered in Maxwell's equations:

$$\nabla \cdot \boldsymbol{E} = \frac{\rho}{\epsilon_0} \tag{2.1}$$

$$\nabla \cdot \boldsymbol{B} = 0 \tag{2.2}$$

$$\nabla \times \boldsymbol{E} = -\frac{\partial \boldsymbol{B}}{\partial t} \tag{2.3}$$

$$\nabla \times \boldsymbol{B} = \mu_0 \epsilon_0 \frac{\partial \boldsymbol{E}}{\partial t} + \mu_0 \boldsymbol{J} \tag{2.4}$$

The integration domain (Ω) and the boundary conditions define the cavity geometry and material; we will consider only the so called Perfect Electric Conductor (PEC) and the Perfect Magnetic Conductor (PMC) conditions:

$$\text{PEC:} \quad n \times \boldsymbol{E} = 0 \quad n \cdot \boldsymbol{B} = 0 \qquad \text{in} \quad \partial\Omega \tag{2.5}$$

$$\text{PMC:} \quad n \times \boldsymbol{B} = 0 \quad n \cdot \boldsymbol{E} = 0 \qquad \text{in} \quad \partial\Omega \tag{2.6}$$

Considering (2.2) and (2.3) one can apply a very common technique which consists in expressing the electric and magnetic fields using the vector and scalar potentials $\boldsymbol{A}$ and Φ:

$$\boldsymbol{B} = \nabla \times \boldsymbol{A} \qquad \boldsymbol{E} = -\frac{\partial \boldsymbol{A}}{\partial t} - \nabla\Phi \tag{2.7}$$

and the Coulomb gauge is chosen for $\boldsymbol{A}$:

$$\nabla \cdot \boldsymbol{A} = 0 \tag{2.8}$$

By substitution of these two equations in (2.1) and (2.4) and with a few manipulations, it's easy to get the following two equations which are equivalent to Maxwell's equations provided above:

$$-\nabla^2 \boldsymbol{A} + \frac{1}{c^2}\frac{\partial^2}{\partial t^2}\boldsymbol{A} = \mu_0 \boldsymbol{J} - \frac{1}{c^2}\frac{\partial}{\partial t}\nabla\Phi \tag{2.9}$$

$$-\nabla^2 \Phi = \frac{\rho}{\epsilon_0} \tag{2.10}$$

where ∇^2 is the vector Laplace operator.

We consider an empty cavity, without charges and without internal current, so that $\rho = 0$ and $\boldsymbol{J} = 0$. Moreover, for the sake of simplicity we apply only PEC boundary conditions, which imply that the contour surface is equipotential. Therefore the last equation can be left aside since a suitable solution for the scalar potential is, for example, $\Phi = 0$. (2.9) becomes:

$$\nabla^2 \boldsymbol{A} = \frac{1}{c^2}\frac{\partial^2}{\partial t^2}\boldsymbol{A} \tag{2.11}$$

This is a so called wave equation and can it be shown that its solutions may be decomposed into a series of orthogonal functions which is called eigendecomposition ([3]).

$$\boldsymbol{A} = \Re(\sum_{n=0}^{\infty} e^{i\omega_n t}\boldsymbol{A}_n(\boldsymbol{r})) \tag{2.12}$$

Where each term $\boldsymbol{A}_n$ is a solution of the following equation for one specific ω_n

$$\nabla^2 \boldsymbol{A}_n = -(\frac{\omega_n}{c})^2 \boldsymbol{A}_n \tag{2.13}$$

(2.13) is obtained by transforming (2.11) to the frequency domain and is called Helmholtz equation. The $\boldsymbol{A}_n$ are the so called "eigenmodes" and are orthogonal to each other, in the sense that:

$$\forall m, n \quad \int_\Omega \boldsymbol{A}_n \cdot \boldsymbol{A}_m d\Omega = 2\delta_{mn} \frac{\sqrt{U_n U_m}}{\epsilon_0 \omega_n \omega_m} \tag{2.14}$$

where δ_{mn} is the Kronecker delta and U_i is the energy of the mode i. The terms $\boldsymbol{A}_n$ of the decomposition are the eigenmodes and each one of them is a particular solution of the boundary value problem with a fixed angular frequency ω_n: in principle every eigenmode has got its own frequency, which is called eigenfrequency and therefore its own ω_n .

From the vector potential $\boldsymbol{A}$ one can compute the electric and magnetic fields, whose eigendecomposition will be:

$$\boldsymbol{E} = \Re\left(\sum_{n=0}^\infty e^{i\omega_n t} \boldsymbol{E}_n(\boldsymbol{r})\right) \qquad \boldsymbol{B} = \Re\left(\sum_{n=0}^\infty e^{i\omega_n t} \boldsymbol{B}_n(\boldsymbol{r})\right) \tag{2.15}$$

2.1.2 Cylindrically symmetric cavity

When the cavity has a cylindrical symmetry the electric and magnetic fields of each eigenmode can be written in the so called "multi-pole" expansion [4]. For the following equations we use the cylindrical coordinates; let r be the radial distance, θ be the azimuth and z be the axial distance, whereas $\boldsymbol{u}^{\mathrm{r}}$, $\boldsymbol{u}^\theta$ and $\boldsymbol{u}^{\mathrm{z}}$ are respectively the versor of the radial direction, the versor of the azimuthal direction and the versor of the axial direction.

The above mentioned expansion is:

$$\begin{aligned}
\boldsymbol{E}_n = \sum_m [&E_{n,m}^{\mathrm{r}}(r,z)\cos(m\theta)\boldsymbol{u}^{\mathrm{r}} \\
&+E_{n,m}^\theta(r,z)\sin(m\theta)\boldsymbol{u}^\theta \\
&+E_{n,m}^{\mathrm{z}}(r,z)\cos(m\theta)\boldsymbol{u}^{\mathrm{z}}]
\end{aligned} \tag{2.16}$$

$$\begin{aligned}
\boldsymbol{B}_n = \sum_m [&B_{n,m}^{\mathrm{r}}(r,z)\sin(m\theta)\boldsymbol{u}^{\mathrm{r}} \\
&+B_{n,m}^\theta(r,z)\cos(m\theta)\boldsymbol{u}^\theta \\
&+B_{n,m}^{\mathrm{z}}(r,z)\sin(m\theta)\boldsymbol{u}^{\mathrm{z}}]
\end{aligned} \tag{2.17}$$

When considering the electric field components: $E_{n,m}^{\mathrm{r}}$, $E_{n,m}^\theta$, $E_{n,m}^{\mathrm{z}}$, it is common use to talk of monopole modes for $m = 1$, dipole modes for $m = 2$, quadrupole modes for $m = 3$, etc. The same is for the magnetic field components.

2.1.3 R/Q parameter

The main properties of a mode can be expressed by means of some parameters, one of them is the R/Q. In order to define it, we must first define some other figures of merit of a cavity.

The first parameter we define is the "longitudinal" voltage of the $m-$th multipole expansion component of the $n-$th mode with displacement r:

$$V_{n,m}^{\parallel}(r) \doteq \int_0^L E_{n,m}^{\mathrm{z}}(r,z)e^{-i\omega_n z/c}dz \tag{2.18}$$

Where i is the imaginary unit, L is the length of the cavity and c is the speed of light. The real part of $V_{n,m}^{\parallel}(r)$ is the voltage, due to the mode component we are considering, that a particle experiences when transversing the cavity at speed c.

Another parameter is the energy stored in a mode:

$$U_{n,m} \doteq \frac{\epsilon_0}{2} \int_\Omega |\boldsymbol{E}_{n,m}(\boldsymbol{r})|^2 d\Omega \tag{2.19}$$

The parameters that are mostly used to characterize the coupling between a mode and a particle beam transversing the cavity are the loss parameter and the R/Q. The definition for the loss parameter is the following:

$$k_{n,m}(r) \doteq \frac{|V_{n,m}^{\parallel}(r)|^2}{4U_{n,m}} \tag{2.20}$$

Whereas the definition we apply for the R/Q is[1]:

$$R/Q_{n,m} \doteq \frac{1}{r^{2m}} \frac{4k_{n,m}(r)}{\omega_n} \tag{2.21}$$

It can be shown (see [7] and [8]) that the parameter $R/Q_{n,m}$ is independent on the displacement considered when the this displacement is small enough, since $V_{n,m}^{\parallel}(r) \sim r^m$.

---

[1]In literature there are other definitions, a very common one is in [5]. Also the one we chose is largely employed, one reason why we chose it is that its application is simple when the post-processing of CST Studio [6] is employed.

Chapter 3

1.3GHz TESLA Cavity

As already stated, the object of the whole work is to show how Uncertainty Quantification and Sensitivity Analysis have been performed on a TESLA single cell cavity whose fundamental eigenfrequency is 1.3GHz. It is necessary in this framework to explain what the TESLA cavity is and what it is meant for, thus it is unavoidable to give first a short excursus on linear particle accelerators and multicell cavities.

3.1 Multicell cavities in linear accelerators

Advances in particle accelerators are necessary to obtain new advances in particle physics. It is a well known fact, that growing energy particle beams are very important in order to carry out increasingly deeper studies about the fundamental nature of particles.

The technology employable to accelerate particles greatly depends on the type of particle being accelerated. Circular machines are a well established way to accelerate heavy particles like protons, but nowadays there is also a great demand for linear accelerators.

As an example, one reason is given by the fact that, concerning lighter particles like electrons and positrons, interactions in the center-of-mass energy range from 200GeV to more than 1TeV can no longer be studied with circular structures, because of the prohibitive costs due to the synchrotron radiation [9]. Therefore colliders with a linear accelerating structure are required to push further also the research on electron-positron interactions, even if linear accelerators are not limited at all to electrons and positrons.

The best performances in linear accelerators are obtainable with Superconducting Radio Frequency machines. In these machines, particle beams are accelerated while passing through radio frequency cavity resonators which are cooled down to a temperature of 2K [9], where an electric field ringing with an established frequency transmits energy and momentum to the particles. Generally, in electron-positron colliders, the accelerating cavities are

microwave cylindrically symmetric resonators made with numbers of single cells connected one after the other to obtain a "multicell cavity". An example of multicell cavity is provided in Figure 3.1 whereas in Figure 3.2 a section of an accelerating structure is presented.
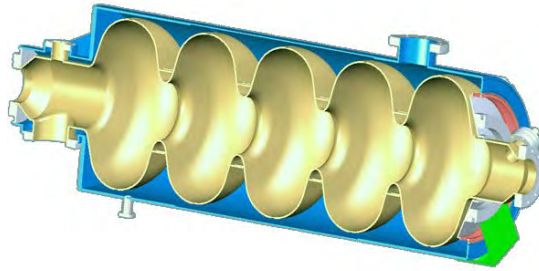

Figure 3.1: A five-cell, $\beta = 1$ elliptical cavity, operating at 704MHz, and optimized to accelerate protons with an energy of around 1GeV, designed by SACM [Courtesy of Irfu]

In order to avoid confusion from now on, when not specified, we will use the word cavity only to refer to the single cell, while we will explicitly say multicell cavity when referring to a series of cells.

Pumped vacuum is present in the cavities and connecting tubes allow the beam pass through several accelerating devices without exiting from the protected atmosphere.
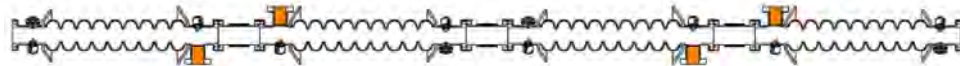

Figure 3.2: String of cavities in ACC39 mounted at FLASH (Picture reprinted from [10])

The fundamental mode of a cavity, which is the one with the lowest frequency, is excited from an external power source and is used to accelerate the particle beam, which passes on the cavity axis. When referring to only one cell that mode is the TM_{010}, also called simply "monopole" mode. Its electric field is longitudinal on the axis and decays when approaching the walls of the cavity. The magnetic field is azimuthal and it is zero on the beam axis.

Both the phase and the frequency of the fundamental mode are extremely important for the accelerating process to work properly. The ideal condition would be the one in which each particle enters the cavity when the electric field is zero in the whole cell, then, when the particle is in the middle of the cavity, the field should have the correct sign in order to transmit a kick in the correct direction and it should be at its maximum, finally the particle

should exit the cavity when the field is zero again and is about to change sign. As the beam is actually passing through a multicell, the TM_{010} mode of the cell immediately after must be excited with a phase shifted of π with respect to the phase of the field in the previous cell. In this way a particle exiting a cell and entering the next one finds again a field pushing it forward.

If the frequency of the field is not the correct one, the passage of the beam trough the cavity takes longer or shorter time than what required for the field to reach its next zero point, this results in phase errors for the other cells and the total accelerating gradient is lower than the desired one. As an extreme condition it can also be negative. For this reason a tuning process is required, which may be done by applying some pressure on the cavity to make it slightly change its shape and volume and therefore its fundamental frequency. In modern particle accelerators the so called blade tuners are often used [11].

Now we must point out that, due to the fact that a multicell cavity is composed by several single cells, talking of the eigenmodes of the whole multicell makes sense while it would not be allowed to consider separately the modes of the cells, because they obviously couple with each other. In a multicell, the acclerating mode is not a TM_{010} but a TM_{01x} where x depends on the number of cells. As the phase shift between the accelerating fields in two subsequent cells must be π, the accelerating mode is usually called "π-mode".

3.2 Geometry of the TESLA cavity

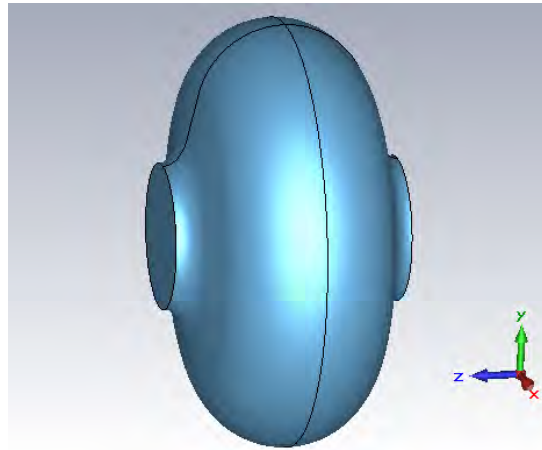Figure 3.3 shows a CST Studio model of the studied TESLA Single-cell.

Figure 3.3: TESLA cavity modelled in CST Studio [Courtesy of J. Heller]

It is composed by two axisymmetric half-cells, which are called "cups".

TESLA cells are usually part of multicell cavities, for instance the 9-cell cavity shown in Figure 3.4.

Figure 3.4:   A 1.3-GHz TESLA-type nine-cell cavity [reprinted from http://newsline.linearcollider.org]

In these devices the first and the last cells of the series are not symmetrical with respect to their welding axis; in addition, also the initial and final cups are different from each other: these design choices were taken to prevent the trapping of higher order modes [9]. Thus we must distinguish between "midcup","endcup1" and "endcup2". In this work only the former has been considered, as we studied a TESLA midcell, which is made by two identical midcups.

The most common way to parametrize a half-cell is shown in Figure 3.5, where also the names for the shape parameters are defined, and their values can be found in Table 3.1.
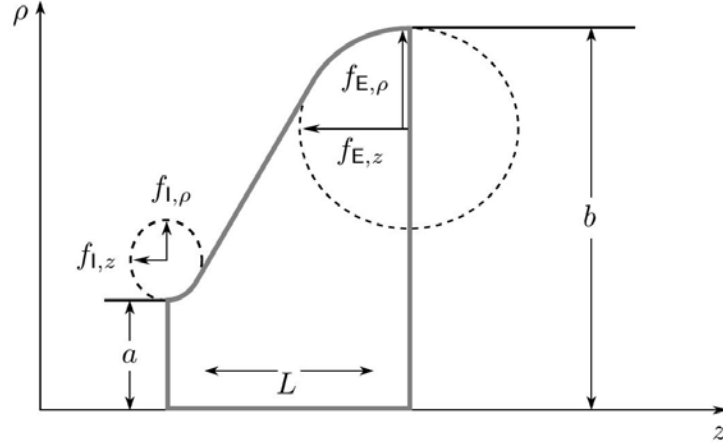

Figure 3.5: Contour and parametrization of a TESLA half-cell [courtesy of Christian Schmidt]

cavity shape parameter	midcup[mm]	endcup1[mm]	endcup2[mm]
equator radius b	103.3	103.3	103.3
iris radius a	35	39	39
equator vertical axis f_{Ez}	42.0	40.3	42
equator horizontal axis $f_{E\rho}$	42.0	40.3	42
horizontal half axis f_{Iz}	12	10	9
vertical half axis $f_{I\rho}$	19	13.5	12.8
length L	57.7	56.0	57.0

Table 3.1: 1.3GHz TESLA half-cell shape parameters [9].

3.3 Eigenmodes in TESLA cavity

As explained before the importance of the TM_{010} mode is due to the fact that it is excited to accelerate the particle beam. Another eigenmode on which we focus is the TM-like$_{110}$, as its level of excitement in real life cavities can be evaluated by the Beam Position Monitor to assess the beam displacement from the ideal direction. The reason is that this mode can only be excited by a displaced beam, and the energy the beam leaves in the mode is monotonic increasing with its distance from the cavity axis. We will call this mode simply TM_{110} even though it would not be allowed, since its magnetic field is not really transversal to the longitudinal direction. Often, when no misunderstanding is possible, this mode is simply called "dipole" mode.

3.3.1 Boundary conditions for the eigenmode solutions

The electromagnetic problem of the cavity is not totally defined until the boundary conditions are completely specified. The superconducting metallic contour of the resonator is modeled in our situation with PEC boundary conditions, instead the beam ports of the cavity need a deeper discussion.

If we imagine that the single cell we are studying is an element of the nine-cell cavity, we ought to chose these conditions in consistency with which electromagnetic aspect we want to examine in the whole device. When we are interested in the π-mode, we chose a boundary condition which imposes the same field on the boundary as what there would be if the cavity were part of the complete nine-cell resonator.

Since in the π-mode the electric field is supposed to be zero on the surfaces between two cells, PMC conditions are chosen on the ports, as in this specific geometry they force the field to have this behavior.

When the study is targeted at the dipole mode, the choice of the bound-

ary conditions for the ports is less easy, because there are several modes in the full multicell corresponding to field configurations in the cells that resemble the TM_{110} mode. A really more rigorous study would be to compute the field in the whole nine-cell cavity, but this is totally unfeasible with the computational power available. Therefore two situations have been studied: one with both the ports with PMC conditions, and another one with both the ports with PEC conditions.

3.3.2   Monopole mode

The field configurations will be explained mostly by means of images containing plots obtained with the Eigenmode Solver of CST Studio. Further informations about the mesh convergence and the settings of the solver can be found in section 5.3.

In chapter 2 we developed the study of the eigenmodes with respect to the magnetic flux density and the electric field, but since CST directly computes the magnetic field strength, this is what we provide in the plots. However, as the material is the vacuum and we are only interested in the shape of the field lines and in the relative amplitude of the vectors, watching at the profile of the magnetic field strength is the same as watching the magnetic flux density.

For the sake of simplicity, from now on we will refer to the plane orthogonal to the axis of symmetry and which splits the cavity in two equal halves as "transversal" plane, instead a plane containing the axis of symmetry of the cavity will be given the adjective "longitudinal".

The TM_{010} mode of the TESLA cavity strongly resembles its homologous in the pillbox cavity, and has got rotational symmetry. For the TM_{010} the electric field stays on longitudinal planes, and the magnetic field wraps around the electric field lines, and so it is always orthogonal to these planes. Figures 3.6, 3.7, 3.8, 3.9 show the field configurations.

As it is clear also from the plots, in the multipole expansion of this mode, only the monopole component is present. Therefore when studying the coupling between the mode and a beam passing through the cavity the monopole definition of the R/Q is chosen (for the definition see section 2.1.3).
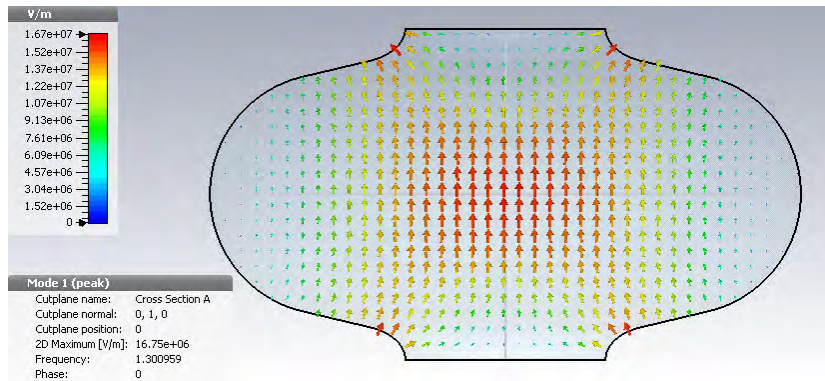
Figure 3.6: Longitudinal section of TESLA cavity, electric field of TM_{010} mode with PMC conditions on the ports.
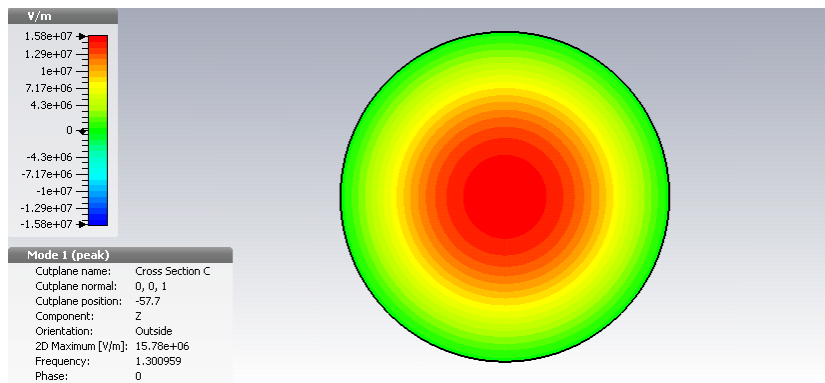

Figure 3.7: Transversal section of TESLA cavity, electric field in axial direction of TM_{010} mode with PMC conditions on the ports.
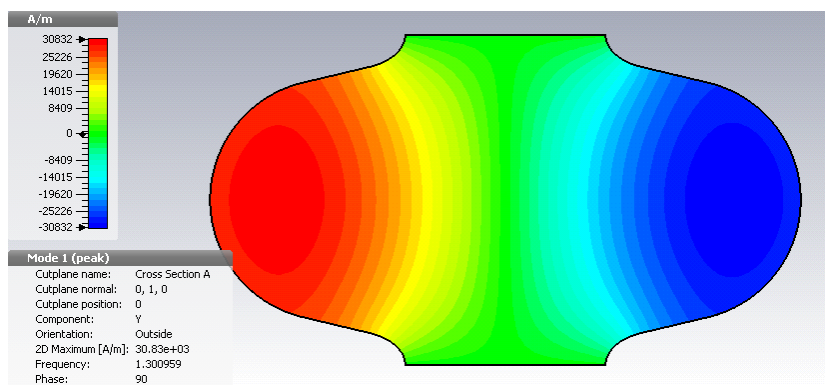

Figure 3.8: Longitudinal section of TESLA cavity, magnetic field strength orthogonal to the cut of TM_{010} mode with PMC conditions on the ports.
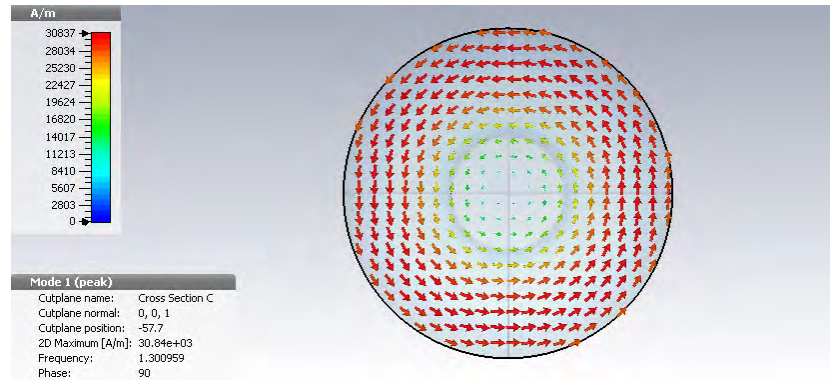
Figure 3.9: Transversal section of TESLA cavity, magnetic field strength of TM_{010} mode with PMC conditions on the ports.

3.3.3 Dipole mode

As one would expect, also the TM_{110} mode in the TESLA cell resembles the corresponding eigenmode in the pillbox cavity. It obviously has got two possible polarizations and we choose only one of them. Regarding the plots that are here provided and the conventions on the symbols and cross sections, we refer to section 3.3.2.

The dipole mode is not axisymmetric but we provide some images with the same cross sections as for the TM_{010}; we have chosen the angular position of the longitudinal cross section where the magnetic field is orthogonal to that very plane and the electric field stays on the plane. The field configuration obtainable with PMC conditions on the ports are presented in Figures 3.10, 3.11, 3.12, 3.13. Whereas Figures 3.14, 3.15, 3.16, 3.17 show the fields with PEC conditions on the ports.

For the mode TM_{110} the dipole component of the multipole expansion is absolutely the main one while the monopole component is exactly null. Therefore when studying the coupling between the mode and a beam passing through the cavity the dipole definition of the R/Q is chosen (for the definition see section 2.1.3).

Figure 3.10: Longitudinal section of TESLA cavity, electric field of TM_{110} mode with PEC conditions on the ports.

Figure 3.11: Transversal section of TESLA cavity, electric field in axial direction of TM_{110} mode with PEC conditions on the ports.

Figure 3.12: Longitudinal section of TESLA cavity, magnetic field strength orthogonal to the cut of TM_{110} mode with PEC conditions on the ports.

Figure 3.13: Transversal section of TESLA cavity, magnetic field strength of TM_{110} mode with PEC conditions on the ports.
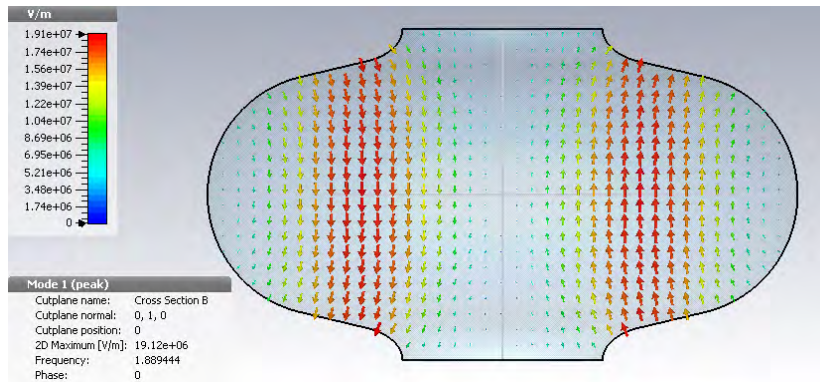
Figure 3.14: Longitudinal section of TESLA cavity, electric field of TM_{110} mode with PMC conditions on the ports.
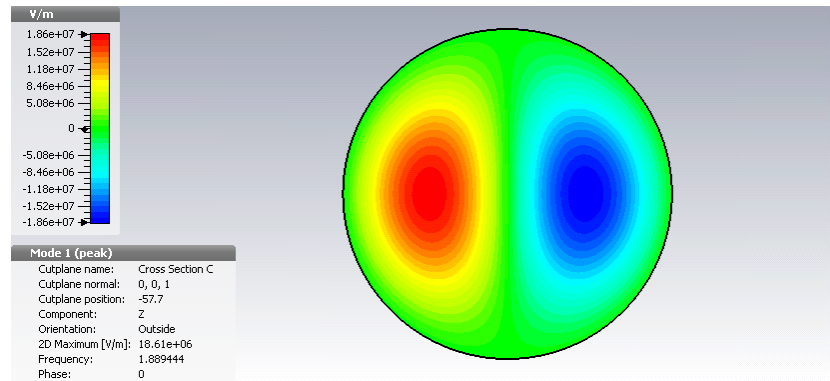

Figure 3.15: Transversal section of TESLA cavity, electric field in axial direction of TM_{110} mode with PMC conditions on the ports.
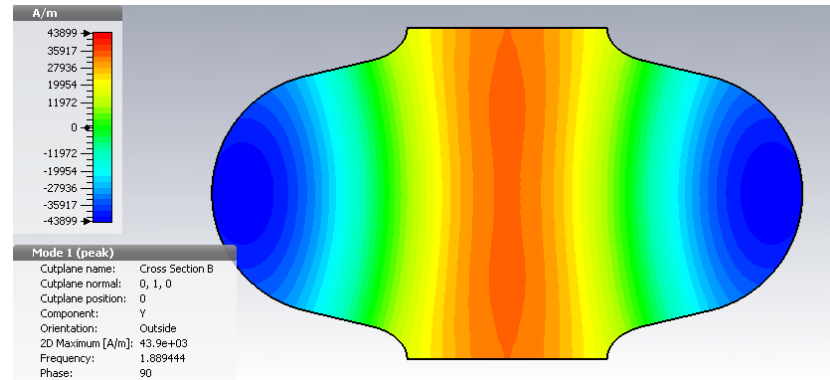

Figure 3.16: Longitudinal section of TESLA cavity, magnetic field strength orthogonal to the cut of TM_{110} mode with PMC conditions on the ports.
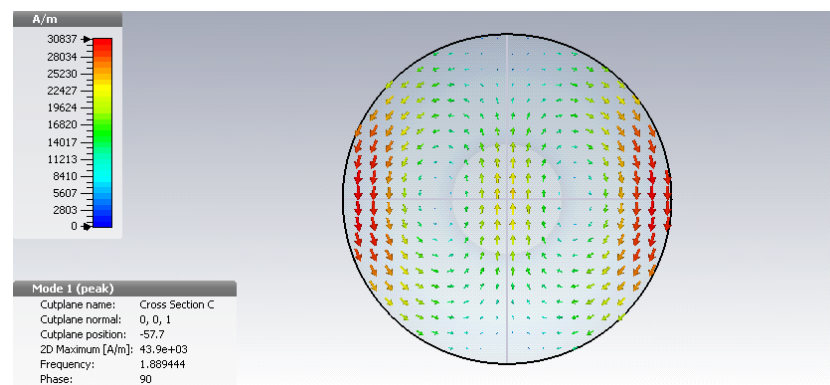
Figure 3.17: Transversal section of TESLA cavity, magnetic field strength of TM$_{110}$ mode with PMC conditions on the ports.
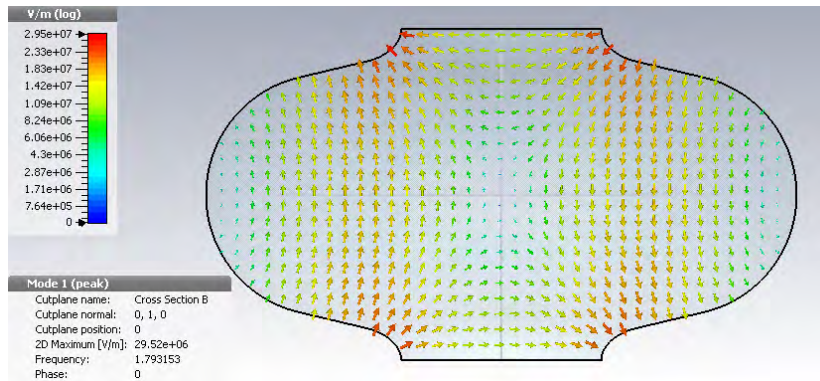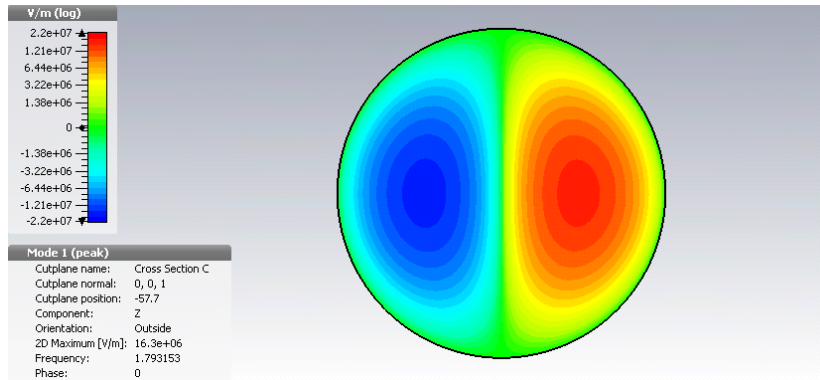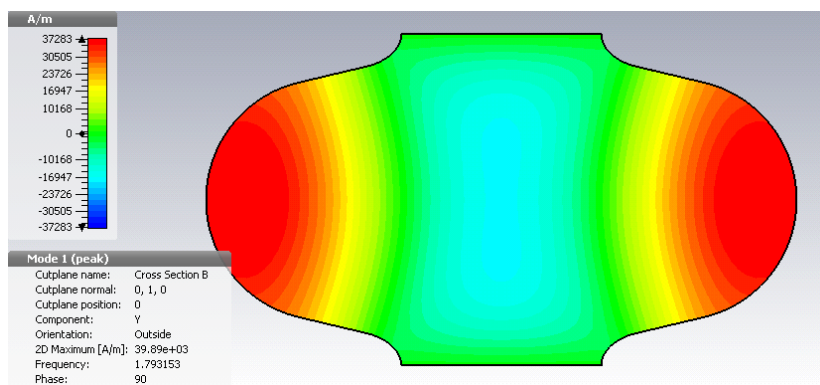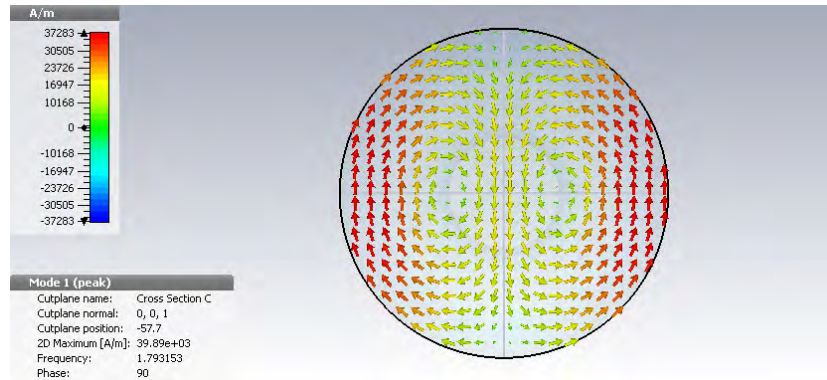
Chapter 4

Methods for Uncertainty Quantification

While studying a complex system, it might be required to give an estimation of the effect of the uncertainty in the input parameters, on the uncertainty of the output of the system. This is the purpose of the Uncertainty Quantification (UQ). A further step in the study consists in apportioning this uncertainty, quantitatively or qualitatively, to the different parameters given as input [12]. This is the goals of Sensitivity Analysis (SA).

In general such analysis can be viewed as the study of a function of the form:

$$\boldsymbol{y} = f(\boldsymbol{x}) \tag{4.1}$$

where the vectors $\boldsymbol{x} = (x_1, x_2, ..., x_p)$ and $\boldsymbol{y} = (y_1, y_2, ..., y_m)$ represent the input parameters to the model and the various outputs. It often happens that $\boldsymbol{x}$ and $\boldsymbol{y}$ are of high dimension. From now on, in order to simplify the description only a scalar output for the function f is considered.

Given the uncertainty of the input vector $\boldsymbol{x}$, doing UQ usually means estimating the cumulative distribution function of the output y:

$$\mathrm{CDF}_y(Y) \doteq \mathrm{prob}(y \leq Y) \tag{4.2}$$

Also some stochastic moments (like the mean value $\mu(y)$ and the variance $\mathrm{Var}(y)$) and the probability density function (pdf) of the output value are evaluated. Here are their definitions, the last two expressed also in form of expectations:

$$\mathrm{pdf}_y(Y) \doteq \frac{d\mathrm{CDF}_y}{dY} \tag{4.3}$$

$$\mu(y) \doteq \int_R Y \mathrm{pdf}_y(Y) dY = \mathbb{E}[y] \tag{4.4}$$

$$\mathrm{Var}(y) \doteq \int_R (\mu(y) - Y)^2 \mathrm{pdf}_y(Y) dY = \mathbb{E}[(y - \mu)^2] \tag{4.5}$$

Moreover it's possible to evaluate some quantiles. A p-quantile ξ_p of the random variable y is the smallest Y such that

$$\text{prob}(y \leq Y) \geq p \qquad p \in (0, 1) \tag{4.6}$$

One thing worth to be noted is that the 0.5-quantile has got a special name: it is called "median".

Of course the p-quantile can be defined also using the inverse of the CDF_y, as:

$$\text{CDF}_y^{-1}(p) = \xi_p \tag{4.7}$$

The uncertainties of the input parameters must be known in advance; it's also possible to take into account various correlations and relationships between them. In case no correlation exists between to different parameters and no further cross relations are considered, the uncertainty in the input is given as a set of cumulative distribution functions, one for each element in $\boldsymbol{x}$:

$$\text{CDF}_{x_1}, \text{CDF}_{x_2}, .., \text{CDF}_{x_p} \tag{4.8}$$

Sensitivity analysis is instead more complicated to define, since it involves the determination of the effects of the individual input on the output of the system and several measures of this kind are available. A very common approach consists in viewing SA like an analysis of variance problem. In this case the variance of the output is decomposed into components due to the individual input parameters; the size of each component provides a measure of the importance of the corresponding variable. Figure 4.1 shows the schematic and intuitive idea of what is UQ and SA. It's worth to note

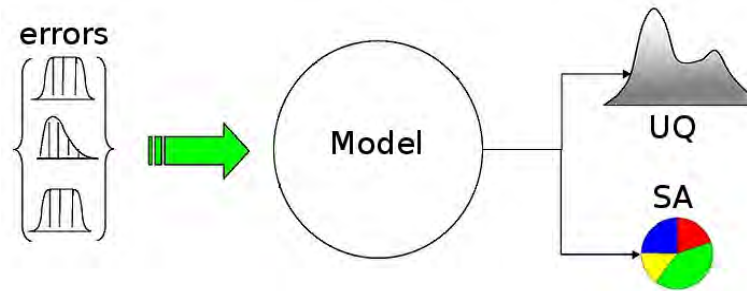Figure 4.1: SA and UQ scheme [reprinted from: "Sensitivity scheme" by Andrea Saltelli - I created this work entirely by myself.. Licensed under Public domain via Wikipedia http://en.wikipedia.org/wiki/File:Sensitivity_scheme.jpg#mediaviewer. . . . . ./File:Sensitivity_scheme.jpg]

that typically the function f is not known analytically and it is rather expensive to evaluate (e.g. in terms of money or time or also technologically

challenging), since performing an evaluation of y usually involves running computer simulations or physical experiments. For this reason it is very important to minimize the number of evaluations of the model required for UQ and SA.

4.1 Monte Carlo methods

Monte Carlo (MC) is a family of probabilistically based techniques used to estimate the quantities above. These methods are widespread in particle dynamics, fluid dynamics and other fields like financial mathematics. As their formal purpose is to estimate integrals, MC approaches are not limited to UQ but this is the context in which we present it.

The idea is to develop a map of the function f by sampling the input space and evaluating the model in those points. Let a sample be:

$$\boldsymbol{x}_i = (x_{i1}, x_{i2}, .., x_{ip}), \quad i = 1, 2, .., N \tag{4.9}$$

where N is the size of the sample and represents the number of points taken from the input space, and p is the dimension of the input space. The sample has to be taken in consistency with the pdf of the input parameters. The specific sampling procedure changes depending on which of the MC methods is chosen.

Evaluating the model in the sample elements we create the following mapping (from analysis inputs to results):

$$[\boldsymbol{x}_i, y_i \doteq f(\boldsymbol{x}_i)], \quad i = 1, 2, ..., p. \tag{4.10}$$

For UQ purposes, the CDF, the mean and the variance of the output are computed with estimators whose expression changes depending on the sampling technique used. For SA, a straightforward approach consists in building a multilinear approximation of the model:

$$\hat{y} = b_0 + \sum_{j=1}^{p} b_j x_j \tag{4.11}$$

whose coefficients b_j are measures of importance of input parameters. Of course this technique does not perform well when applied to highly non-linear systems. Another quick way to assess the relationships between the x_i and y is to visually examine the scatterplots:

$$[x_{ij}, y_i], \quad i = 1, 2, ..., N \tag{4.12}$$

and look for evident patterns, crowded regions or other behaviors that show a certain correlation between the parameter considered and the output.

Before looking at the specific sampling techniques, we define what we mean by rate of convergence of a MC method. Provided that the standard

deviation of a quantity computed with MC (Q) has got the asymptotic behavior:

$$\text{Std}(Q) \longrightarrow \frac{\lambda}{N^c} \qquad \text{when} : N \to \infty \tag{4.13}$$

where λ is a constant, the rate of convergence is the constant coefficient c.

4.1.1   Simple Random Sampling

One way of sampling for MC techniques is the so called "Random Sampling"; in literature this method is also referred as "Simple Random Sampling" or "Crude Monte Carlo". We will refer to Monte Carlo with Random Sampling with the acronym "RS".

This strategy is the simplest one; in case of non correlated input parameters it consists in generating each sample element independently from the others. Let

$$r_{i,j}, \qquad i = 1, 2, .., N, \;\; j = 1, 2, ..p, \tag{4.14}$$

be $N \times p$ independent and identically distributed numbers sampled from $\text{Unif}[0, 1)$, the RS sample elements are:

$$\boldsymbol{x}_i = (\text{CDF}_{x_1}^{-1}(r_{i1}), \text{CDF}_{x_2}^{-1}(r_{i2}), .., \text{CDF}_{x_p}^{-1}(r_{ip})), \quad i = 1, 2, .., N \tag{4.15}$$

Estimators

After proceeding with the sampling, the model is evaluated in order to obtain the y_i. Than it is possible to estimate the CDF of the output according to:

$$\hat{\text{CDF}}_y(Y) \doteq \frac{1}{N} \sum_{i=1}^{N} \text{H}(Y - y_i) \tag{4.16}$$

where H refers to the Heaviside step. The mean value of y is approximated with the estimator:

$$\hat{\mu}_y \doteq \frac{1}{N} \sum_{i=1}^{N} y_i \tag{4.17}$$

whereas we can approximate the variance with:

$$S_y^2 \doteq \frac{1}{N-1} \sum_{i=1}^{N} (\hat{\mu} - y_i)^2 \tag{4.18}$$

The estimators (4.16),(4.17) and (4.18) are unbiased[1] when applied with Monte Carlo Random Sampling.

Regarding the pdf of the output, generally providing a good approximation is not as easy as for the CDF; in fact obtaining it as a derivative of the

---

[1]An estimator is unbiased if the difference between its expected value and the value being estimated is null.

CDF is usually not advisable, since (4.16) provides a staircase approxima-
tion of the cumulative distribution. Often the approach of a "kernel density
estimator" is employed in order to have a smooth-looking pdf; as a matter of
fact, this technique has the drawback that one might not have any argument
to justify the choice of the setting parameters for the algorithm.

Another approach is to approximate the pdf by means of histograms. To
build them, first of all the range of values of the y_i is subdivided in several
segments of the same length. Secondly the y_i are cast in different bins ac-
cording to which of the segments of the output interval they belong to. There
will be a single histogram for each bin, whose hight is directly proportional
to the number of elements in the bin itself. Finally the complete diagram is
drawn, sorting the single histograms in ascending order according to which
segment of the range of values of the y_i they refer to.

For the estimation of the quantiles it's enough to invert the CDF_y. It
can be done by sorting the y_i in ascending order as:

$$y_{i_1} < y_{i_2} < ... < y_{i_N} \tag{4.19}$$

then writing with $\lceil \cdot \rceil$ the round-up function, an approximation of the inverse
of the cumulative distribution function of y is:

$$\hat{\mathrm{CDF}}_y^{-1}(p) \doteq y_{i_{\lceil pN \rceil}} \tag{4.20}$$

Confidence interval

It is obviously important, in every numerical method, to be able to provide
an error estimation on the computed quantities. With RS it's possible to
compute a confidence interval (CI) for the estimation of the mean value. A
CI of confidence level $L\%$ for a computed parameter $\hat{\mu}$ is an interval which
is calculated by sampling a population, and it is such that when several
samplings of the same population are done and a CI of confidence level $L\%$
is estimated every time and for the same parameter, L% of these CIs contain
the true value of that parameter.

Given a set of independent and identically distributed variables:

$$y_i, \quad i = 1, 2, ..., N \tag{4.21}$$

when N is very high, a CI on confidence level $\kappa \cdot 100\%$ can be built on their
sample mean $\hat{\mu}_y$ [13]:

$$[\hat{\mu}_y - \mathrm{z}(\frac{1+\kappa}{2})\frac{S_y}{\sqrt{N}}, \hat{\mu}_y + \mathrm{z}(\frac{1+\kappa}{2})\frac{S_y}{\sqrt{N}}] \tag{4.22}$$

where $\mathrm{z}(\beta)$ is the β-quantile the Normal distribution and S_y is the sample
standard deviation, defined with:

$$S_y \doteq \sqrt{\frac{\sum_{i=1}^{N}(y_i - \hat{\mu}_y)^2}{N-1}} \tag{4.23}$$

It is clear that the convergence of RS does not depend on the dimension of the input space [2], though some other weird effect may pop up when the dimension is too high with respect to the sample size.

Furthermore, the reader is invited to notice that RS is a technique whose convergence is guaranteed and always has the same rate, but unfortunately it is quite slow, since it is equal to 0.5 . For instance, in order to halve the width of the CI, keeping the same confidence level, the number of evaluations of the model has to quadruple.

4.1.2   Latin Hypercube Sampling

Another option to perform the sampling for a MC technique is the Latin Hypercube Sampling (LHS), which is a special case of Stratified Sampling. To generate a LHS sample of size N the interval $(0, 1)$ is subdivided in N disjoint and equally long sub-intervals. Then 1 point per each sub-interval is randomly chosen to generate the vector:

$$\boldsymbol{l}_1 = (l_{11}, l_{21}, ..., l_{N1}) \quad i = 1, 2, .., N \tag{4.24}$$

This process is repeated p times, to generate the matrix

$$\boldsymbol{l} = \begin{bmatrix} l_{11} & l_{12} & \ldots & l_{1p} \\ \vdots & \ddots & & \vdots \\ l_{N1} & \ldots & & l_{Np} \end{bmatrix}$$

After that, for each column of this matrix a random permutation is performed on its elements (the permutations must be independent from each other). Finally the sample is obtained by defining the vectors:

$$\boldsymbol{x}_i = (\text{CDF}_{x_1}^{-1}(l_{i1}), \text{CDF}_{x_2}^{-1}(l_{i2}), .., \text{CDF}_{x_p}^{-1}(l_{ip})), \quad i = 1, 2, .., N \tag{4.25}$$

Estimators

For the LHS some of the same estimators as for RS are available but some distinctions are necessary. (4.16),(4.17) and (4.20) still are unbiased estimators of the same quantities for which they had been defined, but (4.18) is not.

When LHS is applied, for the variance there is no unbiased estimator; we used the following one:

$$S_{y,\text{LHS}}^2 \doteq \frac{1}{N} \sum_{i=1}^{N} (\hat{\mu} - y_i)^2 \tag{4.26}$$

---

[2]This is a good property that instead does not hold for several other methods. Some of them suffer instead of the so called *curse of dimensionality*, which means that the required sample size scales with the dimension of the input space

However, in the worst case its bias will not be higher than $1/N$, because the following holds for LHS:

$$\frac{N-1}{N}\text{Var}(y) \leq \mathbb{E}[S^2_{LHS}] \leq \text{Var}(y) \qquad (4.27)$$

when $y = f((x_1, x_2, ..., x_p))$ is monotonic in each of the x_i [14].

Considerations on LHS

From an intuitive point of view the sampling technique applied in LHS is more able to cover the whole input space, providing a more uniform sampling of the input parameters and reducing the entity of clusters and unexplored regions. See figure 4.2 for a comparison between samples obtained with RS and with LHS.
For this reason one might expect that LHS always performs better than RS.
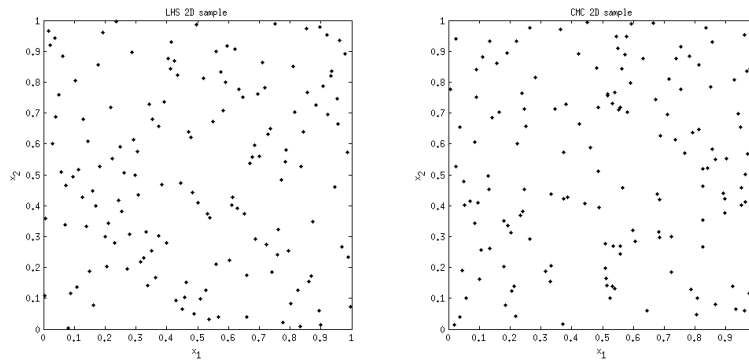
Figure 4.2: RS and LHS samples examples for a 2D input space

In general this is not true as there are several cases where LHS performs the same than RS, and they are not actually very exotic situations. For example, on the model:

$$y = x_1 x_2, \qquad x_1, x_2 \in \text{Norm}(0, 1) \qquad (4.28)$$

LHS has the same convergence rate than RS [15].

Instead LHS clearly beats RS, for the computation of the mean value, when it comes to additive systems where the all the inputs have uniform density functions. Since in these cases its convergence rate on the mean value is 1.5 [16].

Moreover the confidence interval shown for RS does not hold for LHS. The reason is that the sample elements from the input space are correlated. Then no straightforward approach exists to decide a suitable number of sample elements for a specific model.

In addition it is clear that after the sample has been created, its size can't be easily extended to obtain another larger LHS sample which contains

the elements of the previous one. Anyway, there exist some algorithms for extending the size of a sample, (see [17] and [18]), but they change the correlation matrix of the input values; therefore who applies them should know in advance how much the correlation matrix of the input parameters is allowed to change with no appreciable effects on the model behavior.

4.1.3 Replicated Latin Hypercube Sampling

One way to overcome the drawbacks of LHS is to apply a technique which consists in independently generating some LHS samples of the same size. We refer to this method as "Replicated Latin Hypercube Sampling" (rLHS). In literature this name is very common though sometimes it is also used also for different schemes (see [18]).

Iman [19] proposed this technique in 1981. In practice, the idea is to use the results of independent LHS schemes of the same size in order to check how much the output variates from sample to sample; in this way one can compute a CI for several quantities, as it will be explained in the next section.

Confidence interval

Let R be the number of replications, t the size of each LHS sample and y_{ir} the output of the $i-$th sample element of th $r-$th LHS scheme. We define T_r the result of the following estimator on the $r-$th replication:

$$T_r = \frac{1}{t} \sum_{i=1}^{t} g(y_{ir}) \tag{4.29}$$

where g is an arbitrary function, for instance:

- if g is the identity function, then T_r is the sample mean;

- if $g(y) = \mathrm{H}(Y - y)$ for a fixed Y, T_r is an estimate of $\mathrm{CDF}_y(Y)$;

- if $g(y) = y^m$ then T represents the m-th sample moment.

A confidence interval on $\hat{\mu}_T$ of confidence level κ is given by [19]:

$$[\hat{\mu}_T - \mathrm{t}_{R-1}(\frac{1+\kappa}{2})\frac{S_T}{\sqrt{R}}, \hat{\mu}_T + \mathrm{t}_{R-1}(\frac{1+\kappa}{2})\frac{S_T}{\sqrt{R}}] \tag{4.30}$$

In addition to the one provided other confidence intervals for quantiles computed with rLHS may be found in [20] and [21], where also the batching and sectioning techniques are applied.

Cumulative distribution and probability density function

It is important to point out that, by means of the confidence interval provided, it is also possible to place upper and lower uncertainty boundaries on the estimation of the CDF for the output of the model. In fact, chosing a huge number of values for the possible output Y of the model, one can assess the cumulative probability of each one of them with the following estimator:

$$\hat{\text{CDF}}_y(Y) \doteq \frac{1}{Rt} \sum_{r=1}^{R} \sum_{i=1}^{t} \text{H}(Y - y_{ir}) \tag{4.31}$$

Which is nothing else than $\hat{\mu}_T$, where $g(y) = \text{H}(Y - y)$. After that, a CI can be placed around every cumulative probability assessed, which is the same than defining error boundaries around the plot of the CDF.

Leaving aside the uncertainty boundaries and considering only the distribution of the mean values of the cumulative probability, the same approximation of the CDF can be obtained by inversion of the estimation of a sufficiently extended set of quantiles for the output of the model. These quantiles can be computed in a way which is similar to the one employable for RS. All the obtained output values, for every sample element and for every replication, have to be sorted in ascending order as:

$$y_{i_1,r_1} < y_{i_2,r_2} < \cdots < y_{i_{Rt},r_{Rt}} \tag{4.32}$$

than an approximation of any p-quantile ξ_p is:

$$\hat{\xi}_p \doteq y_{i_{\lceil pRt \rceil},r_{\lceil pRt \rceil}} \tag{4.33}$$

where $\lceil \cdot \rceil$ is the round-up function, as already stated. It is intuitive and easy to prove that the inverse of the function $p \mapsto \hat{\xi}_p$ is $Y \mapsto \hat{\text{CDF}}_y(Y)$ [21].

A further important detail is that the estimators provided above, for the CDF and the quantiles, lead to the same results as one would obtain merging together all the output values of the rLHS (as if they were results of a RS scheme of size $N = tR$) and computed the CDF with formula (4.16). Than, since a bijection connects the space of the CDFs with the space of the pdfs, we are allowed to estimate the pdf of the model merging all the replications of a rLHS scheme together and applying the technique of the kernel density or the technique of the histograms, as explained in 4.1.1.

Considerations on the convergence of rLHS

The choice of the size t of each LHS is extremely important in order to reach a desired CI width using the smallest possible number of model evaluations. First of all we make an obvious consideration: when it is known in advance that, for the model under examination, LHS and RS have the same convergence rate, there is no point in applying rLHS, as RS is way more simple and

straightforward to implement. use RS, as in literature are available CI for quantiles when RS is applied, see [20] and [21] . Secondly we note that the choice for the right t may be very challenging; some examples of application of rLHS may be found in literature, but no widely applicable algorithm to decide how to set the method seems to be available. Therefore if no previous knowledge of the model is available, all possible sizes are equally allowed; furthermore: one might fall in a case for which the LHS performs the same than RS, and he probably becomes aware of it when he already has wasted lots of time and model evaluations.

Let us express the CI expression in a more convenient way. Naming $N = Rt$ the number of total evaluations, substituting it in the (4.30) and considering only the half width of the CI, we get:

$$\text{CIhw}_{\text{rLHS}} = \text{t}_{R-1}(\frac{1+\kappa}{2})\frac{\sqrt{t}S_T}{\sqrt{N}} \tag{4.34}$$

We also recall the half width of the CI for RS:

$$\text{CIhw}_{\text{RS}} = \text{z}(\frac{1+\kappa}{2})\frac{S_y}{\sqrt{N}} \tag{4.35}$$

The rate of convergence of rLHS is 0.5, the same than for RS; if the T_r are estimations of the mean value, the difference in terms of performance is in the behavior of $\sqrt{t}S_T$ with respect to the behavior of the standard deviation S_y of the model.
As we said before, if asymptotically LHS has the rate of convergence c, applying rLHS may be worth if $c > 0.5$:

$$\sqrt{t}S_T \longrightarrow \frac{\lambda_{LHS}}{t^{c-0.5}} \leq S_y, \qquad \text{as} \quad t \to \infty \tag{4.36}$$

Since both the expectations on S_y and S_T are almost constant with respect to N when t is fixed[3].

Another thing to take in consideration is the effect of the quantiles of the Student's t-distribution. As $\text{t}_{R-1}((1 + \kappa)/2)$ is noticeably higher than $\text{z}((1 + \kappa)/2)$. Table 4.1.3 shows some values in concern, which have been computed with MATLAB [22].

A clarifying numerical example is now shown. It is the study of the convergence plot of the rLHS for different choices of LHS size, applied to an analytical test case. The results are presented in the plot of Figure 4.1.3.

The test function studied is:

$$y = \frac{x_1 + x_2}{\sqrt{2}}, \qquad x_1, x_2 \in \text{Norm}(0, 1) \tag{4.37}$$

---

[3]They are not exactly constant, since they both represent biased estimators for standard deviations, whose bias depend on the sample size but are decreasing with it.

		κ		
		0.95	0.975	0.99
	2	12.7062	25.4517	63.6567
	3	4.3027	6.2053	9.9248
	5	2.7764	3.4954	4.6041
F	10	2.2622	2.6850	3.2498
	50	2.0096	2.3124	2.6800
	100	1.9842	2.2760	2.6264
	1000	1.9623	2.2448	2.5808

Table 4.1: Values of $\mathrm{t}_{F-1}((1+\kappa)/2)$

The sample sizes used are: 10, 25, 100. The Brute Force Numerics method (see [15] for a short description of the method and for other convergence studies for RS and LHS) has been applied for 50 independent realizations for each LHS size and for each number of replications. The mean value of the CI is plotted and the standard deviation of the CI is presented by means of error bars placed around each CI mean value. The results are presented versus the total number of model evaluations (N).

The plots for different sizes show the same slope (0.5), as the number of replications increases; but they are shifted upwards and downwards with respect to one another, as plots from a higher LHS size have, asymptotically, a smaller intercept.

Another key point is that if a high LHS size had been chosen, when there is the need for another replication, a lot of new model evaluations must be performed. Instead, if the size is small, a little amount of additional evaluations is to be computed every time a new replication is required.

Moreover, it is clear that in some zones the error bars of different convergence plots overlay and this is an indicator that, for certain desired CI widths, more choices for the size can be done. Also, we should remember that the bars represent only the standard deviation of the CI width, and it's possible that the CI obtained with one scheme falls outside from the limits of the error bars. If the distribution of the CI width is normal, only 68% of the widths falls between the two bars.
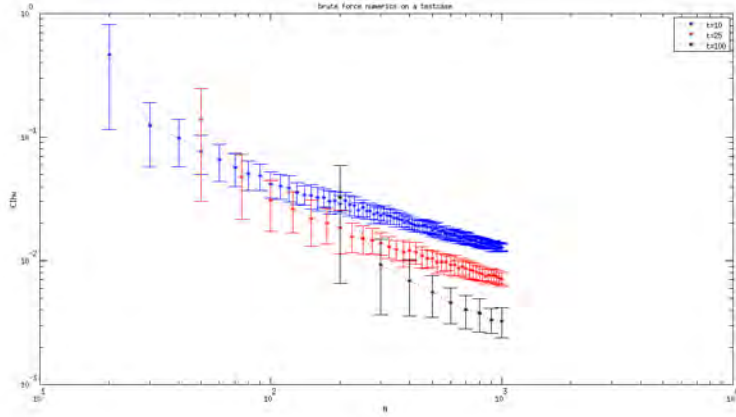
Figure 4.3: convergence plot of rLHS for a test case with different LHS sizes

4.2 Multivariate linear fit for Sensitivity Analysis

An investigation of the mapping in (4.10) can be done with a regression analysis. We recall the expression for a multilinear approximation of the model given in 4.11:

$$\hat{y} = b_0 + \sum_{i=1}^{p} b_i x_i \tag{4.38}$$

The coefficients b_j are what must be determined and they can be used as indicators of the importance of each input parameter x_i on the output uncertainty.

4.2.1 Linear regression coefficients

Once a complete RS or LHS scheme of size N has been completed, it's possible to express the obtained sequence of y_k, $k = 1, 2, ..., N$ using the linear model (4.38):

$$y_k = b_0 + \sum_{i=1}^{p} b_i x_{ki} + \epsilon_k, \qquad k = 1, 2, .., N, \tag{4.39}$$

where the ϵ_k are error terms and are defined with $\epsilon_k = y_k - \hat{y}_k$. In order to determine the b_j it's convenient to use a matrix representation of the last equation:

$$\boldsymbol{y} = \boldsymbol{x}\boldsymbol{b} + \boldsymbol{\epsilon} \tag{4.40}$$

where:

$$\boldsymbol{y} = \begin{bmatrix} y_1 \\ \vdots \\ y_N \end{bmatrix}, \quad \boldsymbol{x} = \begin{bmatrix} 1 & x_{11} & \ldots & x_{1p} \\ \vdots & \vdots & & \vdots \\ 1 & x_{N1} & \ldots & x_{Np} \end{bmatrix}, \quad \boldsymbol{b} = \begin{bmatrix} b_0 \\ \vdots \\ b_p \end{bmatrix}, \quad \boldsymbol{\epsilon} = \begin{bmatrix} \epsilon_1 \\ \vdots \\ \epsilon_m \end{bmatrix},$$

The approach chosen is to minimize the sum $\sum_{k=1}^{N} \epsilon_k^2$. This is called "Least squares approach" and put another way, the b_j are determined in order to minimize:

$$(\boldsymbol{y} - \boldsymbol{x}\boldsymbol{b})^{\mathrm{T}}(\boldsymbol{y} - \boldsymbol{x}\boldsymbol{b}) = \sum_{k=1}^{N}(y_k - b_0 - \sum_{j=1}^{p} b_j x_{kj})^2 = \sum_{k=1}^{N} \epsilon_k^2. \qquad (4.41)$$

By considering the first derivatives of the previous sum and with a little bit of algebraic manipulations the following equation is found, which defines the b_j:

$$\boldsymbol{x}^{\mathrm{T}}\boldsymbol{x}\boldsymbol{b} = \boldsymbol{x}^{\mathrm{T}}\boldsymbol{y}. \qquad (4.42)$$

As the number of model evaluations usually exceeds the number of input parameters, the columns of $\boldsymbol{x}$ are linearly independent and $\boldsymbol{x}^{\mathrm{T}}\boldsymbol{x}$ is invertible, therefore the b_j are obtained with the calculation of:

$$\boldsymbol{b} = (\boldsymbol{x}^{\mathrm{T}}\boldsymbol{x})^{-1}\boldsymbol{x}^{\mathrm{T}}\boldsymbol{y} \qquad (4.43)$$

Furthermore, considering the sample mean and standard deviation of the input parameters x_i and of the output y:

$$\hat{\mu}_{x_i} = \frac{1}{N} \sum_{k=1}^{N} x_{ik}, \qquad S_{x_i} = \sqrt{\sum_{k=1}^{N} \frac{(x_{ik} - \hat{\mu}_x)^2}{N-1}}$$

$$\hat{\mu}_y = \frac{1}{N} \sum_{k=1}^{N} y_k, \qquad S_y = \sqrt{\sum_{k=1}^{N} \frac{(y_k - \hat{\mu}_y)^2}{N-1}}$$

it is possible to reformulate the linear model in equation (4.38) as:

$$\frac{\hat{y} - \hat{\mu}_y}{S_y} = \sum_{i=1}^{p} \frac{b_i S_{x_i}}{S_y} \frac{x_i - \hat{\mu}_{x_i}}{S_i} \qquad (4.44)$$

In literature the so called "Standardized Regression Coefficients" are defined as:

$$\mathrm{SRC}_i \doteq \frac{b_i S_{x_i}}{S_y} \qquad (4.45)$$

It is easy to see that the SRCs are the coefficients that one would find performing the multilinear fit of the model with the input and output normalized in such a way that the have mean value equal to zero and standard deviation equal to one. The coefficient SRC_i provides a measure of how much the output of the system variates (expressed as a fraction of its standard deviation) when the input parameter x_i deviates from its mean value for a certain fraction of its standard deviation. For this reason the SRCs are often preferred to the b_i when sensitivity analysis is performed.

Furthermore, we underline that, differently from the linear model (4.38), the normalized model (4.44) has zero intercept, in fact there is no need to define the coefficient SRC_0 .

4.2.2 Assessing the quality of the fit

Now we would like to have an indicator of the quality of the fit, in order to know how good and reliable the linear model found is in approximating the real mapped model. A help is given by the so called "R square", which we are going to define.

The following relation holds for a least squares regression model:

$$\sum_{k=1}^{N}(y_k - \hat{\mu}_y)^2 = \sum_{k=1}^{N}(\hat{y}_k - \hat{\mu}_y)^2 + \sum_{k=1}^{N}(\hat{y}_k - y_k)^2 \qquad (4.46)$$

In literature the summations above are given the names:

$$\text{SS}_{\text{tot}} \doteq \sum_{k=1}^{N}(y_k - \hat{\mu}_y)^2, \quad \text{SS}_{\text{reg}} \doteq \sum_{k=1}^{N}(\hat{y}_k - \hat{\mu}_y)^2, \quad \text{SS}_{\text{res}} \doteq \sum_{k=1}^{N}(\hat{y}_k - y_k)^2,$$
$$(4.47)$$

where $\text{SS}_{\text{tot}}, \text{SS}_{\text{reg}}, \text{SS}_{\text{res}}$ mean: 'total sum of squares', 'regression sum of squares','residual sum of squares'. It's clear that SS_{res} gives a measure of variability of the regression model with respect to the mapped model. Therefore, the quantity

$$R^2 \doteq \frac{\text{SS}_{\text{reg}}}{\text{SS}_{\text{tot}}} \qquad (4.48)$$

is a measure of the extent to which the linear fit can match the output data. R^2 is simply given the name of "R square" or also "coefficient of multiple determination" and it's always bounded between 0 and 1. The closer R^2 is to the unit, the more appropriate the fit is in accounting for the uncertainty of the model, since at the same time SS_{res} is supposed to approach zero.

Chapter 5

Setting of the problem and numerical approach

The purpose of the work was to perform uncertainty quantification and sensitivity analysis for the R/Q and the frequency of the modes TM_{010} and TM_{110} of the superconducting TESLA single-cell cavity as functions of the geometric parameters. As written in section 3.3.2, for the R/Q of the TM_{010} we chose the definition of the monopole mode, instead we chose the definition of the dipole mode for the R/Q of the TM_{110}, as explained in section 3.3.3.

Here we recall the mentioned definitions:

$$R/Q_{\text{TM}_{010}} = \frac{4k_{\text{TM}_{010}}}{\omega_{\text{TM}_{010}}}, \qquad R/Q_{\text{TM}_{110}} = \frac{1}{r^2}\frac{4k_{\text{TM}_{110}}}{\omega_{\text{TM}_{110}}}$$

where the values are intended for r approaching zero.

We will first describe the details of the stochastic approach chosen for UQ, and especially how the size of the single Latin Hypercube Sampling has been set. Then we will give some informations on the numerical method applied by the software to solve the single cavity problem. Finally we will briefly show how the sampling has been practically implemented with the software tools we employed: CST Studio [6] and MATLAB [22].

5.1 Stochastic approach

As stated before, the rLHS technique was applied to study the effect of the geometric uncertainties on the TESLA cavity.

As presented in section 3.2 each half-cell may be modeled with a set of 7 parameters. Therefore for the whole cell the parameter space has dimension $7 \times 2 - 1 = 13$, because we consider the equator radius only once, in fact the situation in which the two halves have different equator radii would be rather unphysical. Furthermore it is clear that with this parametrization we only consider rotationally-symmetric deviations.

As probability density functions for the input values, Gaussian distributions with relative standard deviation equal to 0.005 were chosen. Their mean values are obviously the nominal values of the parameters.

In other works on Uncertainty Quantification for the single cell cavities (see [2] and [23]), authors decided for different pdfs for the input values, for instance [2] where uniformly distributed parameters with absolute deviations of $\pm 125\,\mu$m were chosen. Since for the deviations we considered it was not possible to find documented data, our choice is motivated by the desire to take a more conservative approach to the UQ and SA for the TESLA cavity. In fact doubling the absolute standard deviations of the distributions chosen, one easily finds that the expected deviations of the parameters from the nominal values are higher than (or in the worst case almost equal to) $125\,\mu$m.

For further informations on the source of the geometric uncertainties in the TESLA cavity see [9].

With this choice of parameters and pdfs, it is intuitive that our model has a certain degree of symmetry and we expect this symmetry to pop up when the sensitivity analysis is performed: the sensitivity indexes of the input parameters are supposed to be equal two by two, except for the one of the equator radius, which does not have any symmetrical counterpart.

5.2 Choice of the size for rLHS

As written in section 4.1.3, the choice of the size for the LHS is very important in a rLHS scheme, since it greatly influences the accuracy that can be obtained with the whole scheme. For our situation, we chose to target the study at the accuracy of the mean values and variances we wanted to compute.

Talking about the accuracy for the output variance is rather difficult since rigorously speaking one is not allowed to apply equation (4.30) and place a confidence interval around its mean value. For this reason we limit our study on the variance to the standard error, rather than applying any confidence interval, even if it is clear that this is not a perfectly meaningful quantity. The expression for the standard error on the estimated mean $\hat{\mu}_T$ of a generic population, sampled R times to obtain the realizations T_r is the following:

$$\text{SE}(\hat{\mu}_T) = \sqrt{\sum_{r=1}^{R} \frac{(T_r - \hat{\mu}_T)^2}{R(R-1)}} \tag{5.1}$$

For the mean values, the problem is simpler, as the computation of a confidence interval is possible.

The requirements are here summarized:

1. half relative width of the CIs on the mean values smaller than 10^{-4} for the frequency and in the range of 10^{-3} for the R/Q ;

2. relative standard error of the computed variances[1] for both the frequency and the R/Q in the range of 10^{-1};

3. relative bias of the estimator of the variances in the range of 10^{-2}.

In order to decide how to satisfy these specifications it would be necessary to know the convergence rate of the LHS for the model studied and the intercept of the convergence plot. The reason is that, once that quantities are known, it is possible to plug them in equation (4.34) and estimate the width of the confidence interval that would be obtained with a certain LHS size; or, which is the same, it would be possible to estimate the total number of samples required to obtain a certain width of the confidence interval with a certain LHS size.

Here we recall that equation, stressing the dependence of S_T on the size t and showing the role of the number of replications R:

$$\text{CIhw}_{\text{rLHS}} = t_{R-1}(\frac{1 + \kappa}{2})\frac{S_T(t)}{\sqrt{R}}$$

Unfortunately, up to now, no clear and reliable idea has ever been provided about the actual performance of the Latin Hypercube Sampling on the model.

As shown in section 3.3.2, the TM_{010} mode of the TESLA cavity is axisymmetric. Thus it is possible to compute it with a 2D code. At our disposal there is SUPERFISH [24] which is a powerful, tool for this task as it is a very performing and accurate 2D code for resonant cavities. In fact, on our workstation (see Table 5.3 for any information on the computer), in less than 15 seconds it is possible to compute the TM_{010} mode with an accuracy several orders of magnitude smaller than the one we would obtain in the same time from a CST 3D solution.

A small brute force numerical approach is therefore affordable with the monopole mode, in order to estimate the convergence rate of the LHS for the mean value of the frequency and R/Q.
In addition, with the data collected by this approach, the estimation of the convergence rate of the standard error on the variances was carried out.

After the estimation of the convergence rate of the LHS for every output parameter is completed, one can give a realistic estimation of the required total number of evaluations for each choice of LHS size, in the study of the TM_{010}. Of course, at this point there would be no need to apply a rLHS

---

[1]However, we are not very strict on this requirement, since from the study of some analytical test cases it is possible to see that very often, also for simple and almost linear functions, the convergence for the variance is extremely poor.

scheme to perform UQ on the TM_{010}, since, from the data computed with brute force numerics, all the questions have been already answered. As a matter of fact, launching a rLHS scheme for the TM_{010} on CST is anyway useful, because we can use it to cross validate the results by comparing the solutions of the two solvers.

However, the key point is that it is considered very likely that the convergence rates of the LHS on the TM_{110} (for both the choices of boundary conditions) and on the TM_{010} are not very different from each other. Thus we apply rLHS on the dipole mode with CST using the same sample size chosen for the monopole mode.

We now show the results of the LHS convergence study.
The brute force numerics was carried out by computing 40 independent realizations of the LHS for each of the different sizes studied: 5,10,40,100. In total $40 \times (5 + 10 + 40 + 100) = 6200$ evaluations were computed, which took less than one day of computational time. The sampling scheme was controlled by a MATLAB script, which for every sample element builds and launches a SUPERFISH script. The file generated by SUPERFISH is then copied by MATLAB in another folder with another name, after that the subsequent sample element is processed. Also the post-processing was done with MATLAB.

The convergence plots obtained are shown in figure 5.1. Blue lines link the dots, which represent the standard deviation estimated for the sizes studied; the red lines represent instead the least squares linear regression of the blue dots. The angular coefficients of the red lines is an estimation of the convergence rate, instead with the intercept we can assess the λ parameter in equation (4.13), since it is equal to $\log \lambda$.

The estimated rates of convergence are provided in Table 5.1

	convergence rate	intercept
$\mu(R/Q)$	0.9503	-2.5967
$\mathrm{Var}(R/Q)$	0.5923	0.2641
$\mu(f)$	1.1156	-2.3661
$\mathrm{Var}(f)$	0.8694	0.3414

Table 5.1: Convergence study results for LHS on TM_{010}.

After these results had been computed, some estimations on the obtainable relative accuracy were performed, by taking in consideration several LHS sizes and numbers of replications. The assessment has been carried out by applying formula (4.34)) with the values for S_T taken from the red line of the convergence plots, and dividing the result by the mean value of the computed quantity. In any case the total number of model evaluations was kept
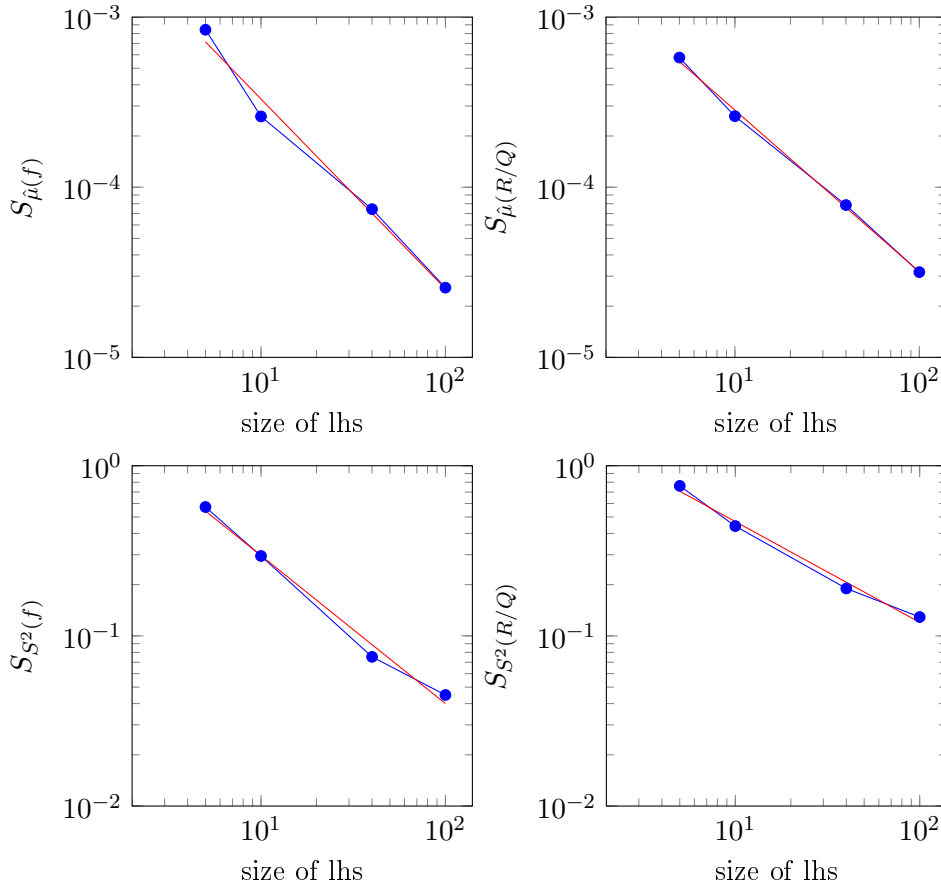
Figure 5.1: Convergence plots of LHS on TM_{010} for the variance and for the mean

below an affordable limit value, which means, considering the computational power available, 800 evaluations.

Several cases for t and R have been taken in consideration, and the final choice was for $R = 5$ and $t = 100$.

In fact for these values of R and t, applying (4.34) means multiplying the S_T obtained from the convergence plots in correspondence to size 100 by the factor 1.24 . One can easily check that in this way we satisfy the first requirement. Furthermore, with size 100 the relative bias of the estimator for the output variance is, in the worst case, 0.01, whereas the expected standard error is very close to the target value.

Moreover, regarding the amount of repetitions, 5 is a number close to the choices made by other authors (see [19] and [25], who chose 3 repetitions). As total number of evaluations, 500 is perfectly affordable.

5.3 Numerical solution of the cavity

Setting properly the 3D code which solves the single cavity problem is extremely important to obtain good results. In fact there is no point in performing UQ when the solution to the single sample has an accuracy not higher than the typical length of th effects one wants to analyze.

In CST Studio a mesh convergence study has been carried out for each output parameter in order to find the best mesh settings and to compare the different solving methods that are available. For the dipole mode part of the study was dedicated to finding the most suitable beam displacement in order to have a good estimation of the R/Q parameter. It is well known that the eigenmode solver of CST applies the Finite Integration Technique when a hexahedral mesh is chosen, while it uses the Finite Element Method with tetrahedral meshes. When solving resonant cavities, it is extremely important to have a very good approximation of the boundary; since CST supports Curved Elements with tetrahedral meshes and Perfect Boundary Approximation with hexahedral meshes, we always applied these settings, with the respective mesh types. The study was performed on the unperturbed cavity, and was based on the a posteriori error; therefore the so called "nominal solution" was computed with growing mesh densities and the convergence plot of the difference between two solutions obtained with two subsequent mesh densities was examined.

The choice between FEM and FIT was done comparing to the computational time, when the same targeted accuracy was reached. In our situation, it was clear that FEM performs better, for both the monopole and dipole modes. The chosen mesh size is such that the number of tetrahedra in the unperturbed structure is 59808.

The nominal solutions together with their estimated accuracies, are shown in Table 5.2.

mode	boundary	output	nominal solution	relative accuracy
TM_{010}	PMC	frequency	1.3009593[GHz]	$\approx 10^{-7}$
		R/Q	113.43[Ω]	$\approx 10^{-4}$
TM_{110}	PMC	frequency	1.793153[GHz]	$\approx 10^{-6}$
		R/Q	0.05881[Ω/mm^2]	$\approx 10^{-3}$
	PEC	frequency	1.889444[GHz]	$\approx 10^{-6}$
		R/Q	0.04808[Ω/mm^2]	$\approx 10^{-3}$

Table 5.2: Nominal solutions of the TM_{010} and TM_{110} in the TESLA cavity.

The transversal beam displacement chosen for the computation of the R/Q of the TM_{110} is 0.8192 mm. During the sampling, a single solution of the

TM_{010} or TM_{110} mode took between 130 and 190 seconds of computational time on our workstation (see Table 5.3), with the settings chosen.

An important detail is that we always applied two symmetry planes for the solutions of the cavity computed during the sampling processes. For the mode TM_{010} we applied magnetic symmetry conditions on two orthogonal planes containing the cavity axis; whereas for the TM_{110} we applied a magnetic symmetry condition on one plane and electric symmetry condition on the other. Obviously these choices led to shorter computational times and made one polarization of the TM_{110} disappear.

No symmetry condition on the plane that separates the two mid-cups was set, since this choice would not have been consistent with the geometric uncertainty we wanted to study; therefore the number of tetrahedra in the mesh of each perturbed structure was around 120000.

5.4   Implementation of the sampling scheme

The rLHS scheme was performed with a workstation whose characteristics are provided in Table 5.3.

CPU	Intel(R)Xeon(R)CPU E5-2687W v2@3.40GHz 3.40GHz
RAM	256GB
OS	Windows Server 2012 Standard

Table 5.3: Characteristics of the machine employed

Regarding the software, the sampling schemes were controlled by a MAT-LAB script. First of all that script creates a VBA macro, which will be used to command CST, than it creates the sample. For each sample element it creates a file with the corresponding values of the input parameters and the VBA macro commands CST to read the input file, which of course changes every time a new element is processed. Before moving to the new sample element, the desired results are withdrawn from the CST result folder and copied to a safe folder.
After the scheme is completed the post-processing is performed with MAT-LAB.

Though CST is an extremely powerful tool for these tasks, in our case study some problems have been encountered while applying the scheme. For example, between 1 and 10 times per each set of 500 eigenmode computations, the solutions provided for the frequency and the R/Q were clearly wrong, being the corresponding values unrealistic; i.e. in the scatterplots these values were strongly displaced with respect to the region where the points corresponding to other sample elements were located. Recomputing the solution of the sample that have had bad results, leads to other values

for the frequency and R/Q, and repeating the computation several times always leads to the same more realistic values for the targeted output parameters. The fact that repeating the simulation several times gives new, but constant and consistent, solutions can be used as a proof that the first result was wrong. Thus, after the scheme was finished, for certain sample elements (the most displaced ones with respect to the rest of the "cloud") it was necessary to repeat the computation.

Chapter 6

Results and discussion

First of all, we will provide the results of the UQ and SA performed. After that a short discussion will be given in order to show how the work outcome meets the expectations and the knowledge already available about the effect of the geometric uncertainties in the model examined.

6.1 Uncertainty Quantification on the Tesla cavity

6.1.1 UQ outcomes for the TM_{010} mode with PMC conditions on the ports

The results for the study of the eigenfrequency and R/Q with the rLHS technique are here provided. In Table 6.1 the mean values are presented together with the relative width of the confidence intervals of confidence level 95% (rel CIhw). In addition to the mean values, the deviations from the nominal solutions are presented.

The reader is invited to pay attention when the accuracy of the nominal solution is not negligible with respect to the half width of the confidence interval[1], since in that case the width of the confidence interval is not a reliable indicator of the error on the mean value. For this reason also the accuracy of the nominal solution is recalled in the table.

However, we are positive that in these situations the order of magnitude of the error can be estimated by summing up the accuracy of the nominal solution and the width of the confidence interval.

Naturally all these considerations apply also to the corresponding results for the dipole mode.

The estimated variances and the corresponding standard errors are provided in Table 6.2

---

[1]We remind that the accuracy of the nominal solution is assumed to be the same of the solution of any of the considered perturbations of the cavity

	frequency	R/Q
mean value	1.300978[GHz]	113.42[Ω]
CI half rel. width	$2.5 \cdot 10^{-5}$	$3.3 \cdot 10^{-5}$
nominal solution rel. accuracy	$\approx 10^{-7}$	$\approx 10^{-4}$
mean-nominal solution	-19[kHz]	$+0.01$[Ω]

Table 6.1: Expected values and deviations from the nominal solution for the eigenfrequency and R/Q of the monopole mode

	frequency	R/Q
variance	$5.61 \cdot 10^{-5}$[GHz^2]	$2.09 \cdot 10^{-1}$[Ω^2]
variance rel. standard error	$3.5 \cdot 10^{-2}$	$7 \cdot 10^{-2}$

Table 6.2: Variances of the eigenfrequency and R/Q of the monopole mode

Moreover, cumulative distribution functions have been estimated for both the R/Q and the frequency. Upper and lower limits of the confidence interval have been computed for every estimated cumulative probability, to give uncertainty boundaries on the plots of the CDFs. The probability density functions have been estimated with both the histograms technique and the kernel density approximation, and they are displayed under the CDFs. These plots are presented in Figure 6.1 and in Figure 6.2.
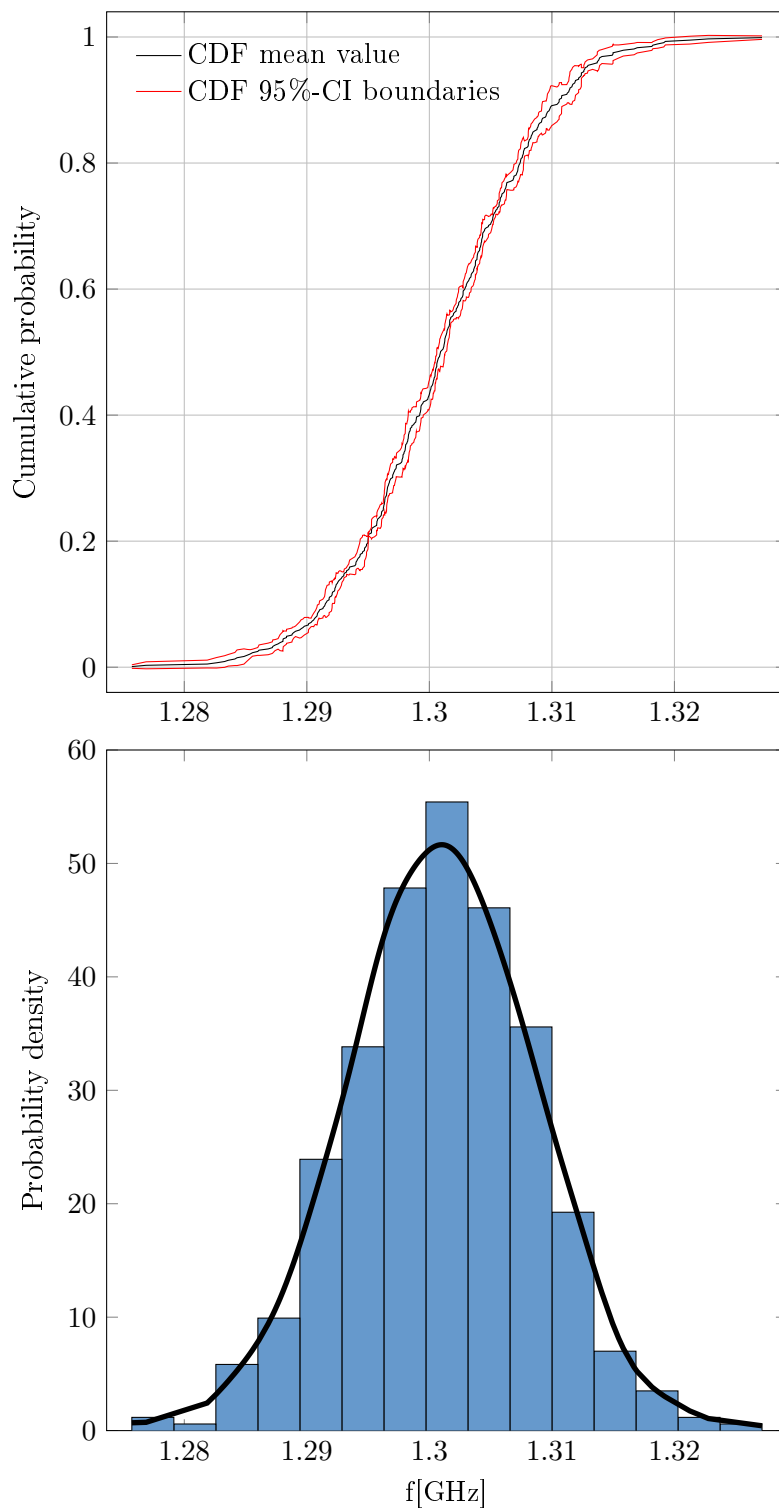
Figure 6.1: Frequency of mode TM_{010} in TESLA cavity: CDF with lower and upper confidence boundaries, pdf approximation with histograms and kernel density (kernel:normal, bandwith:0.00220).
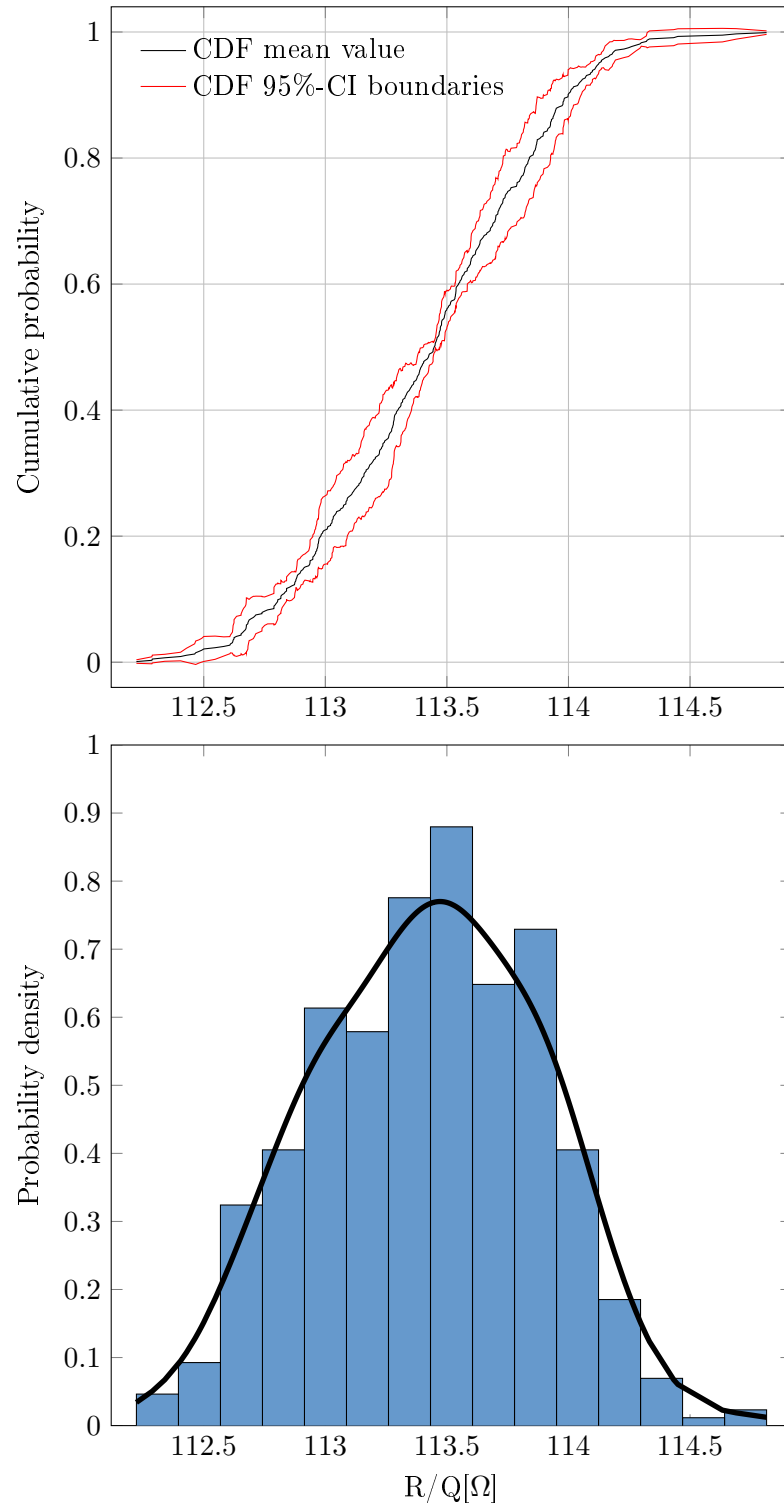
Figure 6.2: R/Q of mode TM_{010} in TESLA cavity: CDF with lower and upper confidence boundaries, pdf approximation with histograms and kernel density (kernel:normal, bandwith:0.159).

6.1.2 UQ outcomes for the TM$_{110}$ with PEC conditions on the ports

Here we present the results for mode TM$_{110}$ of the TESLA cavity with PEC conditions on the beam ports. In Table 6.3 the mean values of the output quantities and their deviations from the nominal solutions are displayed.

The same preliminary considerations on the accuracy as for the monopole mode apply (see section 6.1.1).

	frequency	R/Q
mean value	1.889488[GHz]	48.084 [mΩ/mm^2]
CI half rel. width	$4.4 \cdot 10^{-5}$	$1.3 \cdot 10^{-4}$
nominal solution rel. accuracy	$\approx 10^{-6}$	$\approx 10^{-3}$
mean-nominal solution	-44[kHz]	-4 [μΩ/mm^2]

Table 6.3: Expected values and deviations from the nominal solution of the eigenfrequency and R/Q of the dipole mode, with PEC conditions on the beam ports

The estimated variances and the corresponding standard errors are provided in Table 6.4

	frequency	R/Q
variance	$9.77 \cdot 10^{-5}$[GHz^2]	$4.89 \cdot 10^{-7}$[(Ω/mm^2)^2]
variance rel. standard error	$1.5 \cdot 10^{-2}$	$4.7 \cdot 10^{-2}$

Table 6.4: Variances of the eigenfrequency and R/Q of the dipole mode, with PEC conditions on the beam ports

The estimated CDFs and pdfs for the R/Q and the frequency are provided in Figure 6.3 and in Figure 6.4.
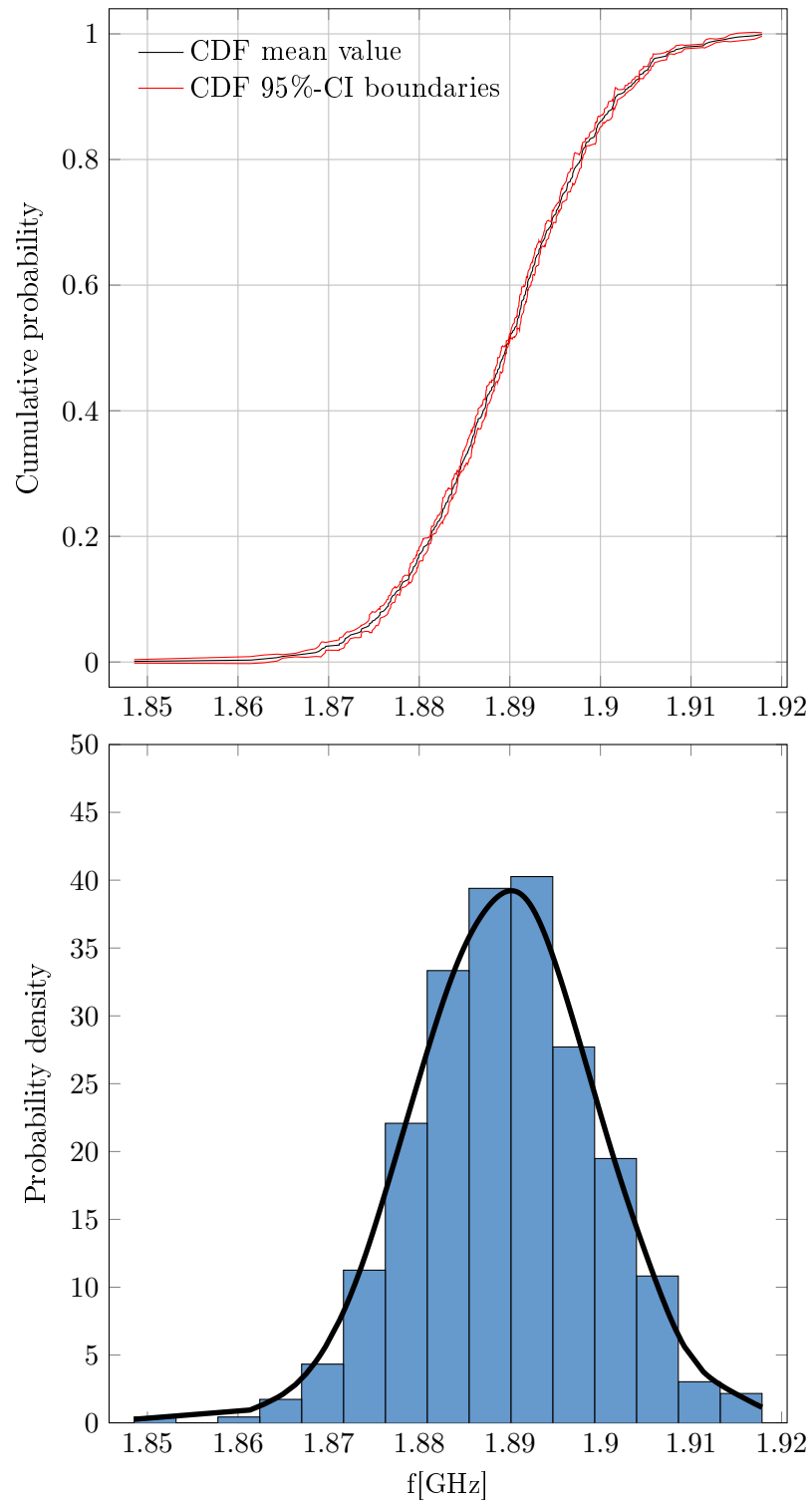
Figure 6.3: Frequency of mode TM$_{110}$ in TESLA cavity with PEC conditions on the beam ports: CDF with lower and upper confidence boundaries, pdf approximation with histograms and kernel density (kernel:normal, bandwith:0.003018).
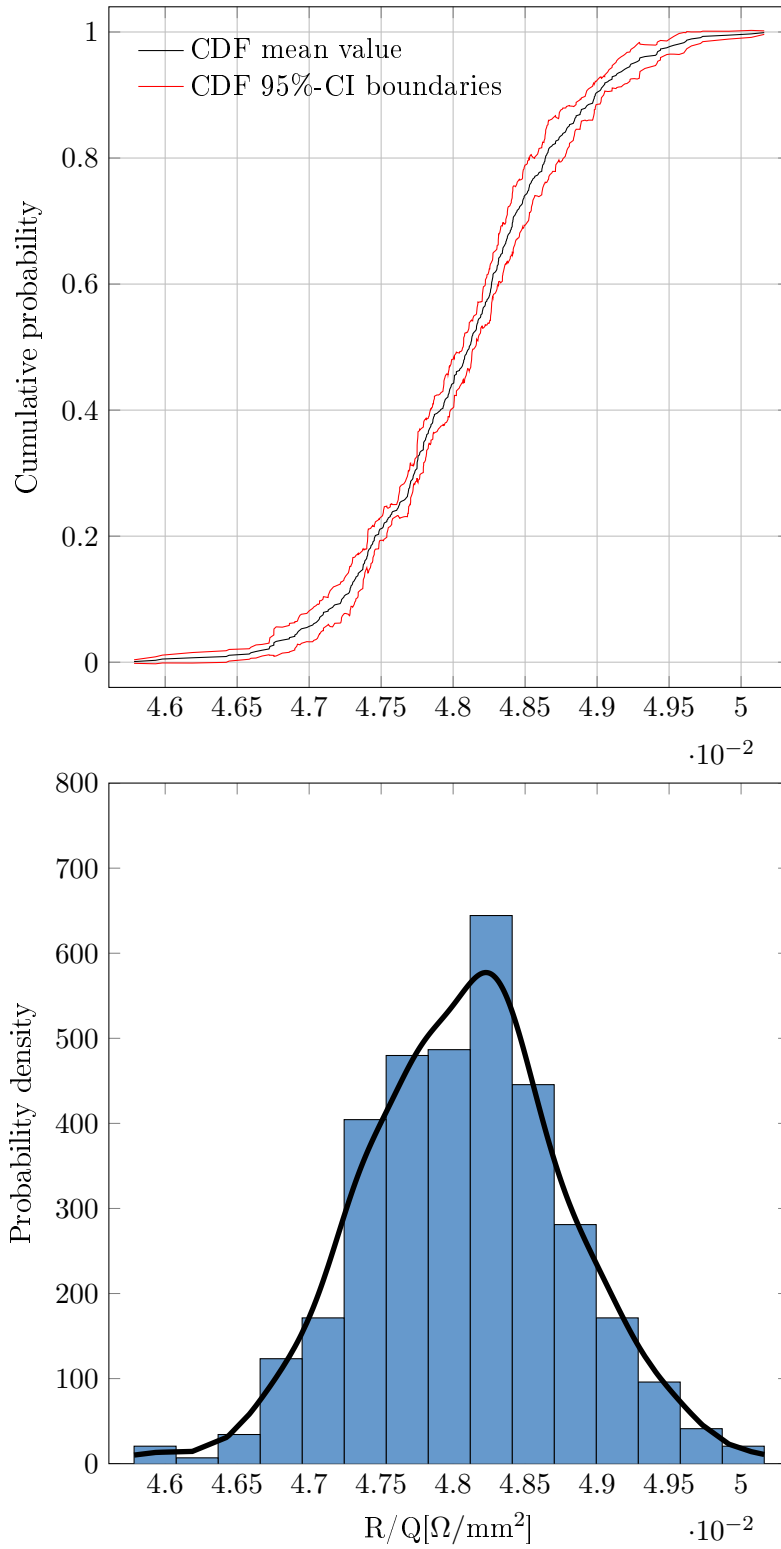
Figure 6.4: R/Q of mode TM_{110} in TESLA cavity with PEC conditions on the beam ports: CDF with lower and upper confidence boundaries, pdf approximation with histograms and kernel density (kernel:normal, band-with:0.0001955).

6.1.3 UQ outcomes for the TM_{110} mode with PMC conditions on the ports

Lastly the results for mode TM_{110} of the TESLA cavity with PMC conditions on the beam ports are presented. In Table 6.5 the mean values of the output quantities and their deviations from the nominal solutions are displayed.

As for the previous situation, about the accuracy, the same preliminary considerations as for the monopole mode apply (see section 6.1.1).

	frequency	R/Q
mean value	1.793163[GHz]	58.852 $[\text{m}\Omega/\text{mm}^2]$
CI half rel. width	$4.4 \cdot 10^{-5}$	$1.9 \cdot 10^{-4}$
nominal solution rel. accuracy	$\approx 10^{-6}$	$\approx 10^{-3}$
mean-nominal solution	-9.7[kHz]	-42 $[\mu\Omega/\text{mm}^2]$

Table 6.5: Expected values and deviations from the nominal solution of the eigenfrequency and R/Q of the dipole mode, with PMC conditions on the beam ports

The estimated variances and the corresponding standard errors are provided in Table 6.6

	frequency	R/Q
variance	$6.34 \cdot 10^{-5}[\text{GHz}^2]$	$3.60 \cdot 10^{-7}[(\Omega/\text{mm}^2)^2]$
variance rel. standard error	$8.6 \cdot 10^{-3}$	$1.9 \cdot 10^{-2}$

Table 6.6: Variances of the eigenfrequency and R/Q of the dipole mode, with PMC conditions on the beam ports

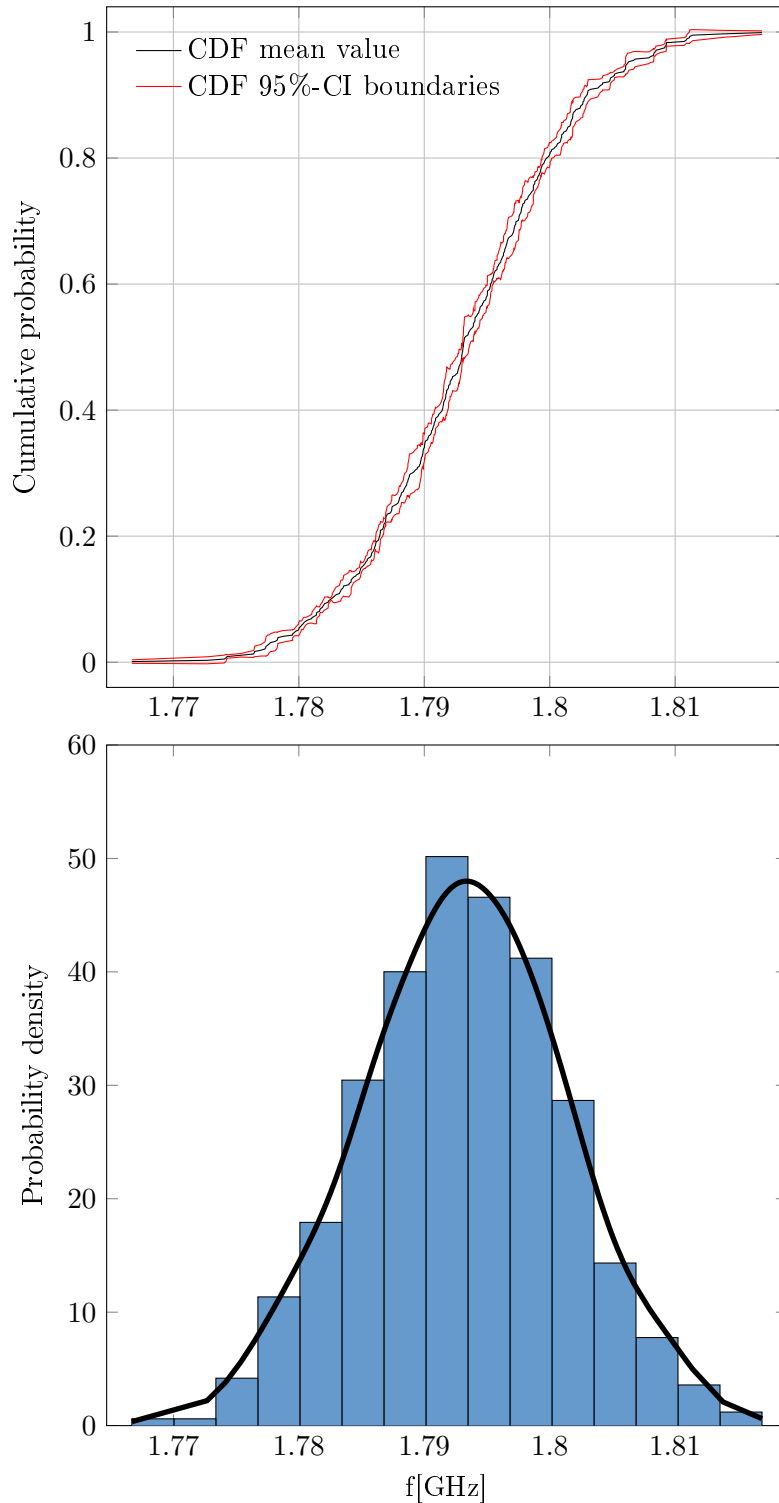The estimated CDFs and pdfs for the R/Q and the frequency are provided in Figure 6.5 and in Figure 6.6.

Figure 6.5: Frequency of mode TM_{110} in TESLA cavity with PMC conditions on the beam ports: CDF with lower and upper confidence boundaries, pdf approximation with histograms and kernel density (kernel:normal, bandwith:0.0025082).
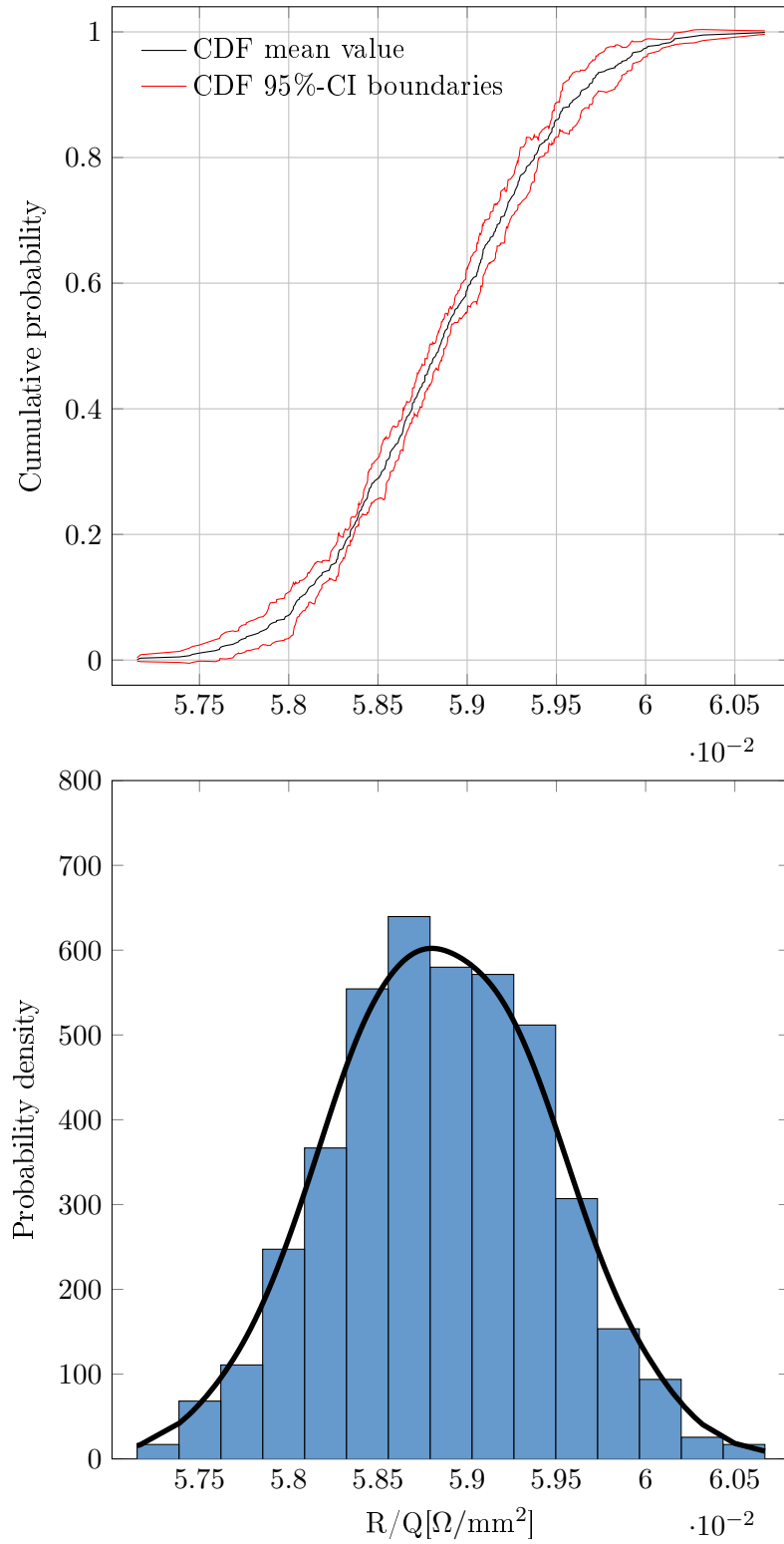
Figure 6.6: R/Q of mode TM_{110} in TESLA cavity with PMC conditions on the beam ports: CDF with lower and upper confidence boundaries, pdf approximation with histograms and kernel density (kernel:normal, bandwith:0.0001932).

6.2 Sensitivity Analysis for the TESLA single-cell cavity

First of all, as sensitivity analysis, the scatterplots were visually examined. Besides the fact that certain parameters show a high correlation with the model outputs, no clusters and neither non-random-looking patterns were found. For this reason we do not provide the scatterplots.

Afterwards a least squares multilinear approximation of the model has been performed for each replication of the LHS and for both the output values. The coefficients of the linear model can be considered as first order sensitivity indices. See section 4.2 for further informations on the multilinear fit of a mapping obtained with a MC technique.

In the linear approximation of the model, the coefficient that multiplies a certain input parameter is an approximation of the partial derivative of the output, with respect to the considered parameter. Than, in order have more meaningful plots, the sensitivity coefficients b_i will be indicated with $\frac{\partial R/Q}{\partial x_i}$ or with $\frac{\partial f}{\partial x_i}$.

The standardized regression coefficients will be instead indicated as "relative sensitivities".

Since at our disposal there are the outputs of 5 replications of a LHS scheme, 5 independent linear fits have been performed per each problem examined and for both the frequency and R/Q. As an error indicator of how reliable our fit is, we computed the standard error of each absolute sensitivity over the 5 replications. Moreover R^2 parameter provides an idea on the level of linearity of our model.

Last but not least, we underline that sensitivity of the output to a parameter located in a certain mid-cup must be almost the same as the sensitivity to the corresponding parameter on the other mid-cup. For this reason, another error indicator is the gap between the sensitivity referring to the parameters of a mid-cup and the sensitivities referring to the corresponding parameters of the other one.

6.2.1 SA outcomes for the TM$_{010}$

We now present the results of the sensitivity analysis for the frequency and the R/Q of mode TM$_{010}$ with PMC conditions on the beam ports.

The width of the absolute standard error is displayed for each sensitivity index as a couple of error bars on top of its histogram.

Figure 6.7 provides the coefficients for the eigenfrequency. Figure 6.8 provides the coefficients for the R/Q of the mode. The R^2 parameters of the linear fits can be found in Table 6.7.
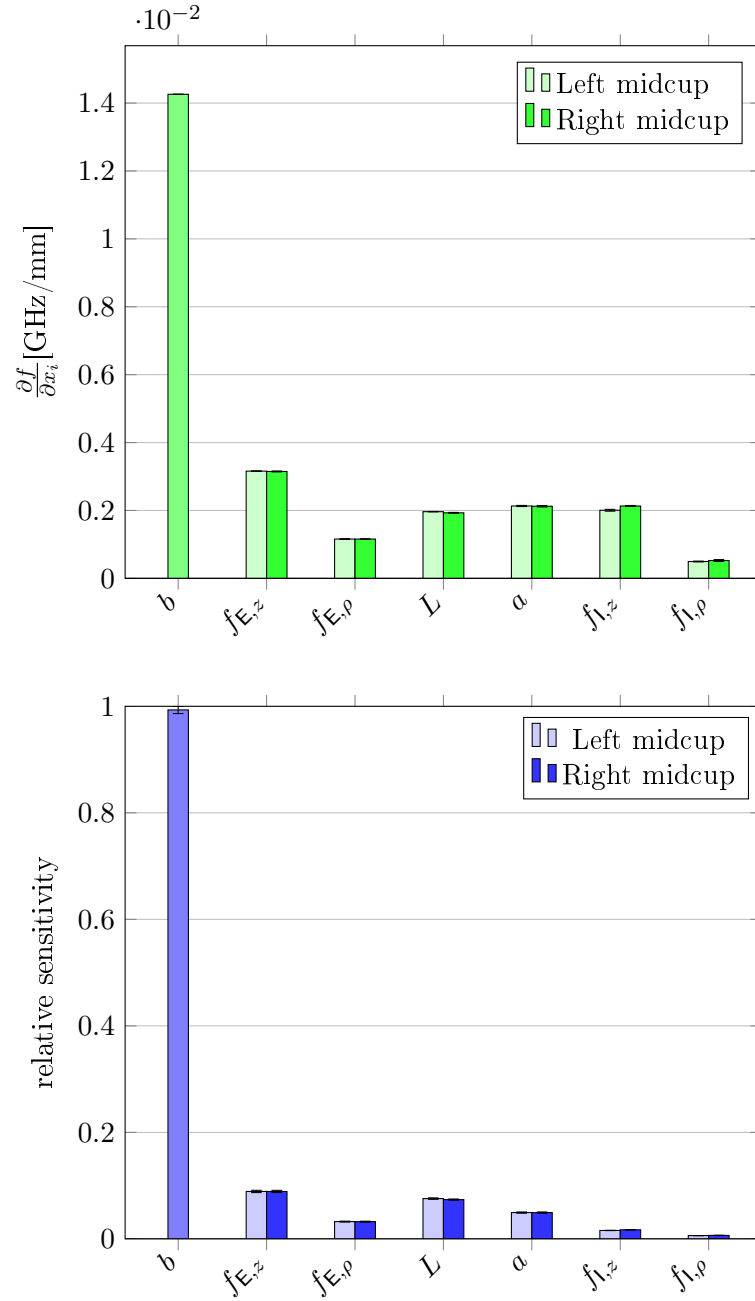
Figure 6.7: Sensitivities for the frequency of mode TM_{010} with PMC conditions on the beam ports
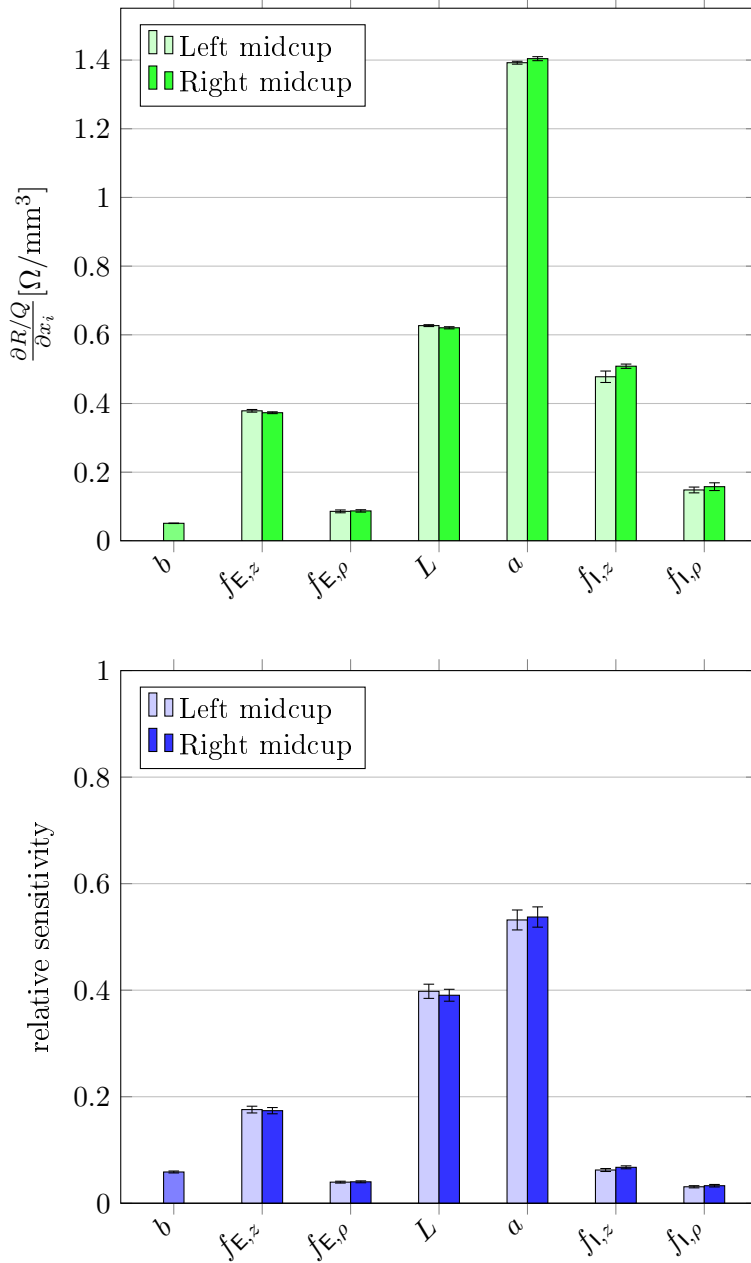
Figure 6.8: Sensitivities for the R/Q of mode TM_{010} with PMC conditions on the beam ports

fit number	frequency	R/Q
1	0.9999	0.9977
2	0.9999	0.9951
3	1.0000	0.9997
4	0.9999	0.9997
5	1.0000	0.9999

Table 6.7: R^2 parameter for the multilinear fits of the mappings for mode TM_{010} with PMC conditions

6.2.2   SA outcomes for the TM_{110} mode

We now present the results of the sensitivity analysis for the frequency and the R/Q of mode TM_{110} with PEC and PMC conditions on the beam ports.

The width of the absolute standard error is displayed for each sensitivity index as a couple of error bars on top of its histogram.

Regarding the solutions with PEC conditions: Figure 6.9 provides the coefficients for the frequency, whereas Figure 6.10 provides the coefficients for the R/Q of the mode. The R^2 parameters of the linear fits can be found in Table 6.8.

For the solution with PMC conditions on the ports: Figure 6.11 provides the coefficients for the frequency, and Figure 6.12 provides the coefficients for the R/Q. Instead in Table 6.9 the values of the R^2 for the corresponding fits are shown.

fit number	frequency	R/Q
1	0.9999	0.9972
2	0.9999	0.9983
3	0.9999	0.9862
4	0.9999	0.9969
5	0.9999	0.9983

Table 6.8: R^2 parameter for the multilinear fits of the mappings for mode TM_{110} with PEC conditions
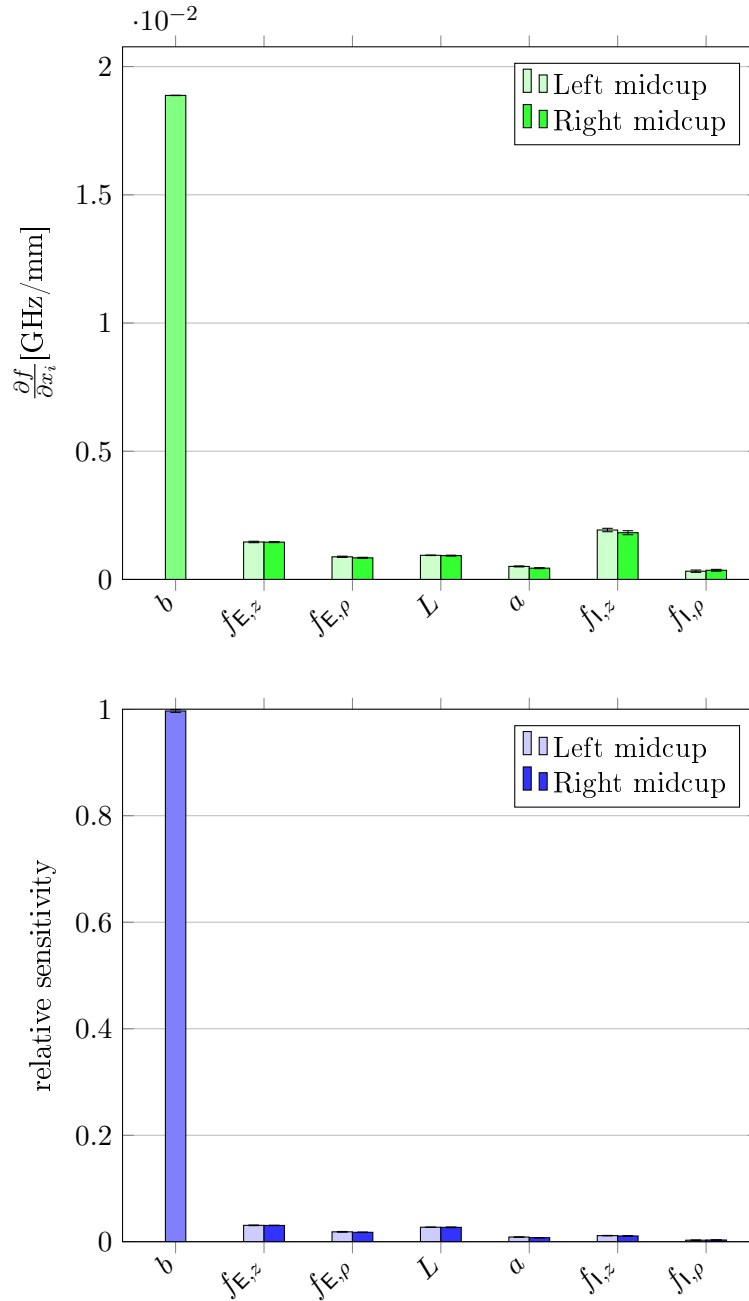
Figure 6.9: Absolute sensitivities for the frequency of mode TM_{110} with PEC conditions on the beam ports
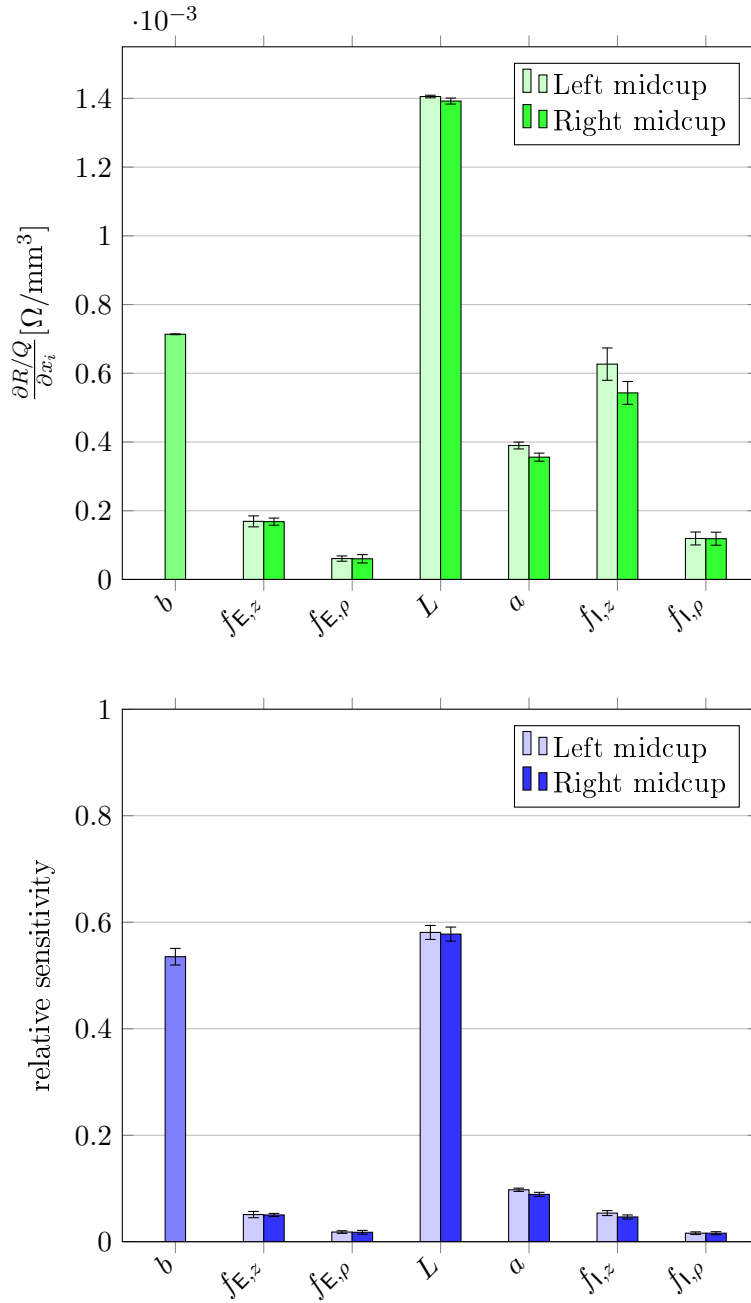
Figure 6.10: Sensitivities for the R/Q of mode TM_{110} with PEC conditions on the beam ports
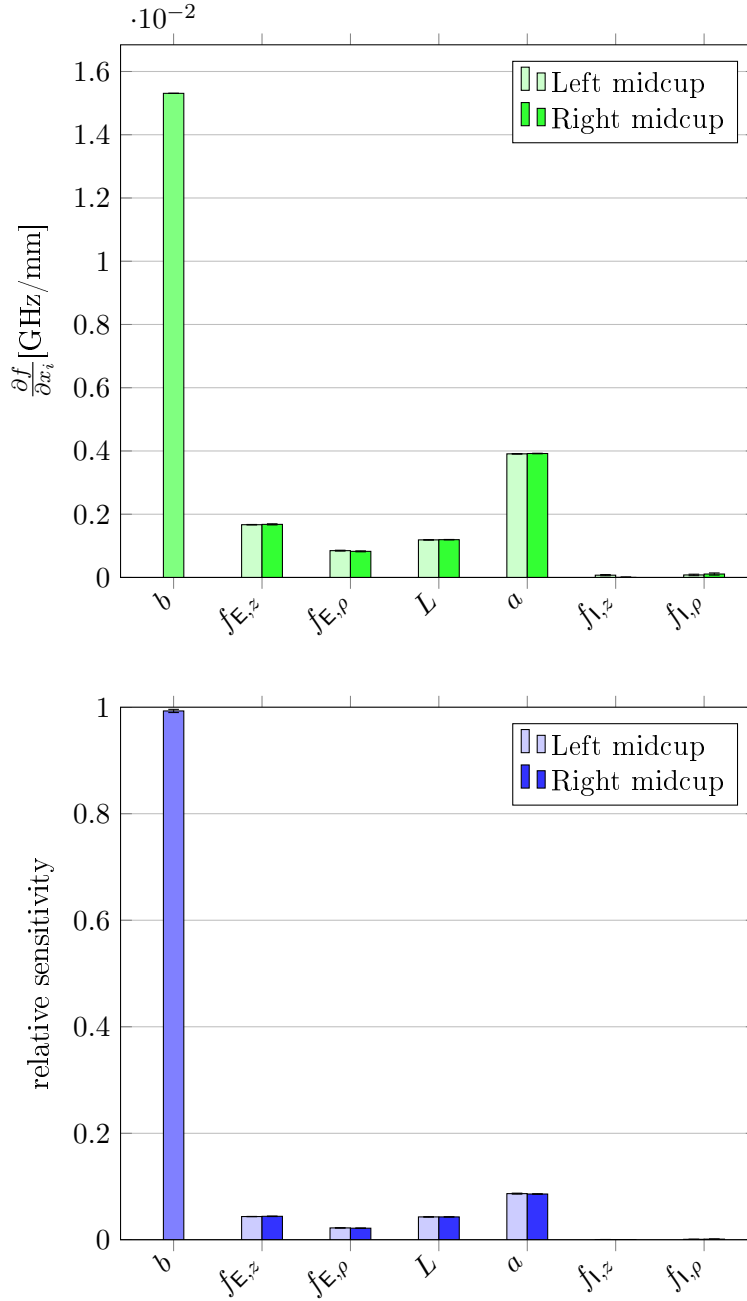
Figure 6.11: Sensitivities for the frequency of mode TM_{110} with PMC conditions on the beam ports
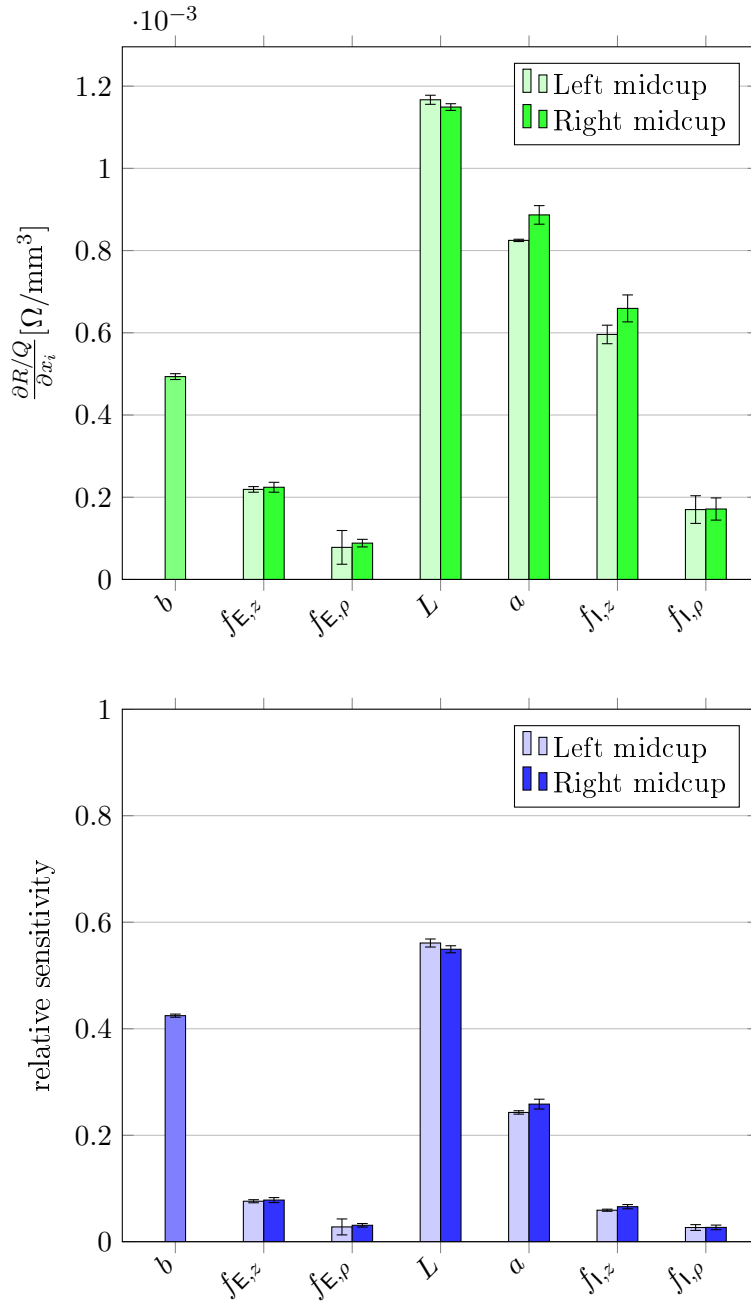
Figure 6.12: Sensitivities for the R/Q of mode TM_{110} with PMC conditions on the beam ports

fit number	frequency	R/Q
1	1.0000	0.9982
2	1.0000	0.9846
3	1.0000	0.9218
4	1.0000	0.9979
5	1.0000	0.9964

Table 6.9: R^2 parameter for the multilinear fits of the mappings for mode TM_{110} with PMC conditions

6.3 Discussion of the results

The UQ and SA performed on the TESLA single-cell cavity has been explained and the results have been provided above.

The specifications for the accuracy of our solutions, given in terms of CI width or standard error, have been met as expected.

The results for the TM_{010} closely resemble what can be found in another study, even though different pdfs for the input parameters were chosen [2].

The applied sensitivity analysis shows that the models we studied are nearly linear, since the minimum R^2 obtained for the linear fit completed is higher than 0.92. Furthermore, the result of the fitting does not variate a lot when it is performed on different replications of the LHS. For these reasons one can say that the approach chosen for SA is perfectly sufficient to estimate the sensitivities of the geometrical parameters.

As a matter of fact a second order polynomial fit is not possible with the sample size chosen, since the linear system that results from the implementation is not overdetermined.

Moreover we have experienced that rLHS is a powerful and reliable technique for the analysis of this kind of problems. What is very important is that the idea about the similar behavior in terms of convergence of the LHS on the monopole and dipole mode was correct. The convergence rate and intercept of the LHS on the monopole mode is close enough to the same convergence rate and intercept of the LHS on the dipole mode to allow us to set the sampling as if we were actually sampling only the monopole mode.

Unfortunately the approach we chose makes sense only when we have a non computationally-demanding system which is expected to have almost the same convergence rate and intercept of the model in which we are mostly interested. In all the other situations, setting properly a rLHS scheme is a non trivial task.

We want to stress that for the problems we studied, applying CMC would

have required an extremely larger sample size in comparison with the number of samples we evaluated with rLHS. For example, since we know the standard deviation of the R/Q parameter of mode TM_{110}, with equation (4.35):

$$\text{CIhw}_{\text{CMC}} = t_{N-1}(\frac{1+\kappa}{2})\frac{S}{\sqrt{N}}$$

it is possible to estimate the number of total samples required with CMC technique to have the same CI width that we obtained with rLHS, which results being 50000.

Lastly, the next step in uncertainty quantification for the TESLA cavity will be to study the effect of geometric uncertainties which allow to consider also non rotationally symmetric deviations.

Bibliography

[1] "CLASSE: SRF.." `http://www.lepp.cornell.edu/Research/SRF/SrfCavitiesAPrimerOne.html#PointOnem`. Accessed: 2014-11-30.

[2] J. Heller, T. Flisgen, E. Brentegani, C. Schmidt, and U. van Rienen, "Quantification of static, geometric uncertainties in superconducting radio frequency cavity cells," *in preparation*.

[3] T. P. Wangler, *RF linear accelerators*. 2008.

[4] T. Weiland, "On the computation of resonant modes in cylindrically symmetric cavities," *Nucl.Instrum.Meth.*, vol. 216, pp. 329–348, 1983.

[5] R. Wanzenberg, "Monopole, dipole and quadrupole passbands of the TESLA 9-cell cavity," 2001.

[6] CST AG, "CST Studio Suite 2014 ®." 64289 Darmstadt, Germany.

[7] T. Weiland and R. Wanzenberg, "Wake fields and impedances," *Lect.Notes Phys.*, vol. 400, pp. 39–79, 1992.

[8] T. Weiland, "Comment on wake field computation in time domain," *Nucl.Instrum.Meth.*, vol. 216, pp. 31–34, 1983.

[9] B. Aune *et al.*, "Superconducting tesla cavities," *Phys. Rev. ST Accel. Beams*, vol. 3, p. 092001, Sep 2000.

[10] E. Vogel *et al.*, "Status of the 3rd harmonic systems for FLASH and XFEL in summer 2008," in *Proc LINAC*, 2008.

[11] R. Paparella, A. Bosotti, C. Pagani, N. Panzer, J. Knobloch, O. Kugeler, and A. Neumann, "Cold Testing And Recent Results of the Blade Tuner for CM2 at FNAL," in *proceedings of PAC09*, (Vancouver,BC,Canada), 2013.

[12] A. Saltelli, K. Chan, and E. Scott, *Sensitivity Analysis*. Wiley series in probability and statistics, Wiley, 2000.

[13] P. Brandimarte, *Handbook in Monte Carlo Simulation: Applications in Financial Engineering, Risk Management, and Economics.* Wiley Handbooks in Financial Engineering and Econometrics, Wiley, 2014.

[14] C. W. Hansen, J. C. Helton, and C. J. Sallaberry, "Use of replicated latin hypercube sampling to estimate sampling variance in uncertainty and sensitivity analysis results for the geologic disposal of radioactive waste," *Procedia - Social and Behavioral Sciences*, vol. 2, no. 6, pp. 7674 – 7675, 2010. Sixth International Conference on Sensitivity Analysis of Model Output.

[15] R. D. Manteufel, "Evaluating the convergence of Latin Hypercube Sampling," *AIAA 2000-1636*, 2000.

[16] R. L. Iman and W. Conover, "Small sample sensitivity analysis techniques for computer models.with an application to risk assessment," *Communications in Statistics - Theory and Methods*, vol. 9, no. 17, pp. 1749–1842, 1980.

[17] C. Sallaberry, J. Heltonb, and S. Hora, "Extension of Latin hypercube samples with correlated variables," *Reliability Engineering and System Safety*, no. 93, pp. 1047–1059, 2008.

[18] J. B. Pleming and R. D. Manteufel, "Replicated Latin Hypercube Sampling," *AIAA 2005-1819*, 2005.

[19] I. Ronald, "Statistical methods for including uncertainties associated with the geologic isolation of radioactive waste which allow for a comparison with licencing criteria," in *Proceedings of the L Symposium on Uncertainties Associated with the Regulationof the Geologic Disposal ofHigh-Level Radioactive Waste* (Kocher DC, editor, ed.), pp. 145–57, 1981.

[20] M. K. Nakayama, "Asymptotically Valid Confidence Intervals for Quantiles and Values-at-Risk When Applying Latin Hypercube Sampling," *International Journal on Advances in Systems and Measurements,*, 2011.

[21] M. K. Nakayama, "Confidence Intervals for Quantiles When Applying Replicated Latin Hypercube Sampling and Sectioning," *???*, ???

[22] MATLAB®, *version 8.2.0.701 (R2013b)*. Natick, Massachusetts: The MathWorks Inc., 2013.

[23] J. Heller, T. Flisgen, C. Schmidt, and U. van Rienen, "Quantification of Geometric Uncertainties in Single Cell Cavities for BESSY VSR Using Polynomial Chaos," Jul 2014.

[24] K.Halbach and R. F. Holsinger, *"SUPERFISH - A Computer Program for Evaluation of RF Cavities with Cylindrical Symmetry"*. Part. Accel.,vol 7, January 1976.

[25] C. W. Hansen, J. C. Helton, and C. J. Sallaberry, "Use of replicated latin hypercube sampling to estimate sampling variance in uncertainty and sensitivity analysis results for the geologic disposal of radioactive waste," *Reliability Engineering & System Safety*, vol. 107, pp. 139–148, 2012.

Acknowledgements